Response to the Reviewers
Format: The reviewers' comments are quoted in italic
Line number in the response refers to the revised manuscript with tracked changes
Quotation in red color stands for revised/added text in the revised manuscript

Overall comment:

We thank the reviewers for their detailed comments. We conducted a substantial revision to the manuscript, including (1) averaging the observations by every 430 seconds (i.e., ~100 km horizontal scale) and comparing them with grid-mean quantities from the simulations (shown in **new Figures 5, 7 to 16**), (2) showing the comparisons of particle size distributions between observations and simulations in **new Figure 4**, and (3) moving the original comparisons between 1-Hz observations and in-cloud quantities of simulations into supplementary material.

Below are our individual responses to the reviewers' comments.

Response to the Reviewer 1's comments:

Review by Andrew Gettelman, NCAR

In general, this is a very well written cutting-edge analysis of a comparison between observations of upper tropospheric ice from aircraft and an advanced large-scale global climate model. However, I have some questions on how the analysis was conducted and the sampling of the models and observations. The work is very cutting edge in the detail of the comparisons, but probably needs a few more pieces of description, and more information perhaps to back up the analysis. I think the manuscript needs some substantial revisions before it will be acceptable for publication in Atmospheric Chemistry and Physics.

Major comments

1) In general, I am concerned that the comparison between the model and observations is not sampling them the same way. It does not seem as if the observations are averaged over a model grid box length before actually reporting values. This should be clarified.

We thank you for this comment and it is a valid concern. Previously, our comparisons were conducted between 1-Hz observations and the in-cloud quantities from CAM6 output (i.e., variables such as "ICINC" and "ICIMR"). That comparison method was similar to the one used in Righi et al. (2020), which compared 1-Hz aircraft observations with in-cloud quantities from simulations of a global climate model (GCM). Considering the suggestion of the reviewer, we use a new method in the main text to compare observations and simulations on more similar scales. This method compares 430-second averaged observations (i.e., ~100 km horizontal scale based on a mean true air speed of ~230 m/s) and grid-mean quantities from the CAM6 simulations. The new comparison results are shown in **revised Figures 5, 7 to 16**. In addition, we moved the original comparisons to supplementary material as **Figures S4, S7 to S12**.

We described the new method in sections 2.2 (line 186 – 194): "In order to examine observations and simulations on more comparable scales, a running average of 430 seconds was calculated for meteorological parameters (i.e., temperature and RHi) and microphysical properties (i.e., IWC, Ni and Di), which translates to ~100 km horizontal scales since the mean true air speed for all campaigns was 230 m/s (supplementary Figure S2). Grid-mean quantities from model output are used in comparisons with observations, including "IWC", "NUMICE", "QSNOW" and "NSNOW", which are mass and number concentrations of ice particles and snow, respectively. Another type of comparison between 1-Hz observations and in-cloud quantities from model output is shown in the supplementary material. Both methods have been previously used in model evaluation, such as D'Alessandro et al. (2019) which compared 200-s averaged aircraft observations with simulated grid-mean quantities, and Righi et al. (2020) which compared 1-Hz aircraft observations with simulated in-cloud quantities."

(line 209 – 211) "In-cloud conditions in simulations are defined by concurring conditions of IWC > 10^{-7} g m^{-3} and Ni > 10^{-4} L^{-1} based on size-restricted grid-mean quantities. These thresholds are the lower limits from observations after calculating the 430-s averages."

2) But fundamentally, when this is done, you get a distribution of individual observations which make up a size distribution. In CAM6, it reports a single mass and number for clouds in a grid box. But this represents a size distribution itself. These size distributions can be compared: it may be that the mass and number is distributed differently than the observations. Gettelman et al 2020, in Press, JGR illustrates this method. You can plot the size distributions from the model by reconstructing the distributions from the model equations.

This is a very helpful comment. We applied the method suggested by the reviewer and reconstructed size distributions for both ice and snow before and after applying the size restriction that excludes ice and snow particles with diameters less than 62.5 μm. We added a **new Figure 4** (below) and more discussions to section 2.2 (line 215 – 220): "To visualize the impact of the size truncation on simulated data, we employed methods similar to Gettelman et al. (2020) and reconstructed the simulated particle size distributions for snow and ice in Figure 4, using gamma functions from Morrison and Gettelman (2008). Note that prior to restricting the diameters of ice and snow particles to ≥ 62.5 μm, the number density for combined ice and snow is overestimated for smaller particles (< 1000 μm) and underestimated for larger particles (≥ 1000 μm). After applying size restriction, the simulated size distribution for combined ice and snow (dashed purple line) becomes more similar to observations due to the reduction of number density of small particles.

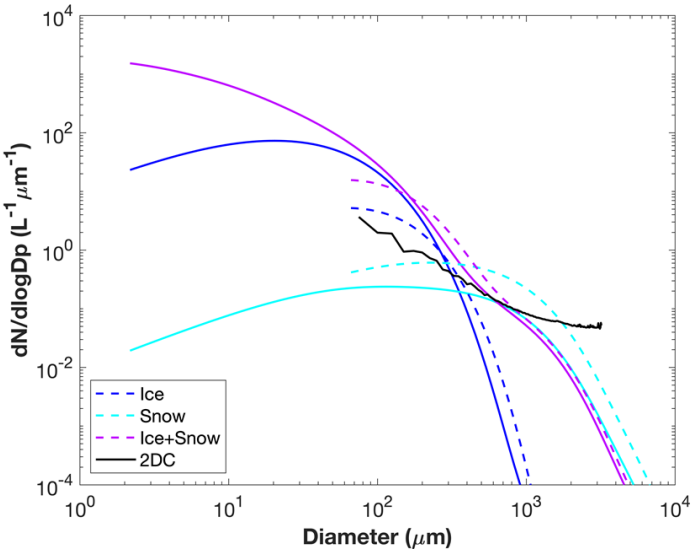

Figure 4. Observed size distribution (black line) and reconstructed size distributions from simulated ice (blue) and snow (cyan). Both full size range (solid lines) and truncated size range of diameters ≥ 62.5 µm (dashed lines) are shown for simulated hydrometeors. Size distributions for combined ice and snow in the simulations (purple) are also shown before and after the size restriction.

References added:

Morrison, H. and Gettelman, A.: A new two-moment bulk stratiform cloud microphysics scheme in the community atmosphere model, version 3 (CAM3). Part I: Description and numerical tests, *J. Clim.*, 21(15), 3642–3659, doi:10.1175/2008JCLI2105.1, 2008.

Gettelman, A., Bardeen, C. G., McCluskey, C. S., Järvinen, E., Stith, J., Bretherton, C., et al. (2020). Simulating Observations of Southern Ocean Clouds and Implications for Climate. *Journal of Geophysical Research: Atmospheres*, 125, e2020JD032619. https://doi.org/10.1029/2020JD032619

3) This leads to my next point. The lack of observations below 62 microns diameter means there may be a significant amount of missing ice in the observations. Have you used the distribution functions to truncate the model size, number and mass to reflect this? If not, it's going to make the comparison even worse. If so, there may be an issue just with the size distributions themselves (see earlier point).

We appreciate you pointing out this issue. To answer your question, the simulated values we used for model evaluation, i.e., IWC, Ni and Di, all reflect the size restriction to ≥ 62.5 µm. To clarify any confusion, we elaborate on our methods for model size constraint in section 2.2 (line 202 – 207): "Simulated ice and snow are restricted to ≥ 62.5 µm based on the size cut-off of the Fast-2DC probe by applying methods from Eidhammer et al. (2014). Based on their equations 1 to 5, we followed their assumption that the shape parameter µ equals 0 when calculating the slope parameter λ. Mass and number concentrations of ice and snow are further calculated based on integrals of incomplete gamma functions from 62.5 µm to infinity. The simulated values of

IWC, Ni and Di are calculated based on the combined ice and snow population after applying the size restriction."

4) I find it hard to imagine that a climate model can produce 30x less ice than observed and still produce reasonable radiative fluxes, particularly for the Outgoing Longwave Radiation. Maybe I am wrong. It's even worse if the model has small ice that is not seen in the observations, but it's explainable if you have removed all the small crystals already. But since you are actually deriving IWC from a distribution of particles, it seems possible that the assumptions you are making may be very wrong (i.e. the number/size v. IWC relationship). What is the uncertainty here? See specific comment below.

We appreciate you pointing out this potential issue. After using the new method of comparing 430-s averaged observations and grid-mean quantities from model output, the differences between simulations and observations become smaller compared with the original method, as shown in revised **Figure 5**. We described these comparisons in section 3.1 (line 238 – 251): "The simulations are further compared with averaged observations at a similar horizontal scale of ~100 km. After applying 430-s running averages for observations, the average IWC and Ni values decrease by 0.5 – 1.5 orders of magnitude compared with 1-Hz observations depending on temperature and geographical region. Hemispheric differences are mostly consistent between 1-s and 430-s averaged observations except for polar regions. … The simulated IWC, Ni and Di also show smaller differences between hemispheres and latitudes. The CAM6-nudg data underestimate and overestimate IWC in the NH and SH by 0.5 – 1 orders of magnitude, respectively, with the largest discrepancies in the midlatitudes. The simulations overestimate Ni in the tropics and polar regions in both hemispheres by 0.5 – 1 orders of magnitude, and overestimate Ni in the southern hemispheric midlatitude by 1 – 2 orders of magnitude. The simulated Di is about half of the observed values in most regions except polar regions."

(line 258 – 260) "A sensitivity test is conducted by comparing 1-Hz observations with in-cloud quantities from model output (supplementary Figure S4). Larger differences are seen between simulated and observed IWC and Ni in Figure S4 compared with Figure 5. The directions (i.e., positive or negative) of model biases of IWC, Ni and Di are generally consistent in both comparisons."

5. Also, there is very little commentary on whether the nudged or free running reproduces observations better. At least not in the conclusions. I think there were some vague comments about the simulations being 'similar'. Is there no appreciable difference?

Thank you for pointing this out. We added discussions of the two types of simulations in the revised manuscript (line 369 – 379): "Comparing the performance of two types of simulations, both CAM6-nudg and CAM6-free show bimodal distributions for IWC – RHi and Ni – RHi correlations, and they both show positive correlations for IWC – σ_w and Ni – σ_w. This result indicates that the general trends in these correlations are statistically robust and less affected by sampling sizes and geographical locations. For correlations with RHi, the maximum IWC value in CAM6-nudg and CAM6-free is lower than the 430-s averaged observations by a factor of 25 and 100, respectively. The maximum Ni value in CAM6-nudg is similar to the 430-s averaged observations, while that value in CAM6-free is lower by a factor of 3. For correlations with σ_w,

there are no significant differences for the maximum IWC between the two simulation types. The maximum Ni value in CAM6-nudg and CAM6-free is higher than the 430-s averaged observations by a factor of 3 and 10, respectively. These results show that CAM6-nudg data, which are collocated with flight tracks, produce IWC and Ni values closer to the 430-s averaged observations than CAM6-free, possibly due to the variabilities of IWC and Ni in different geographical locations as shown in Figure 5."

We also addressed this topic in section 5 (line 430 – 432): "Both simulation types show similar correlation trends of ice microphysical properties with respect to RHi and σ_w. CAM6-nudg performs better for representing IWC and Ni magnitudes than CAM6-free, possibly due to better collocation between CAM6-nudg and observations."

Minor (specific) comments

Page 2, L43: there are IWC observations and compilations that go back decades. Much of it by Heymsfield. Please cite some earlier work.

We addressed this comment by rewording the sentence and adding additional references (line 46 – 48): "In situ observations of tropical, midlatitude, and polar cirrus clouds have shown that IWC can vary orders of magnitude depending on the geographical locations (Heymsfield, 1977; Heymsfield et al., 2005, 2017; Mcfarquhar and Heymsfield, 1997; Schiller et al., 2008)."

References added:

Heymsfield, A. J.: Precipitation Development in Stratiform Ice Clouds: A Microphysical and Dynamical Study, J. Atmos. Sci., 367–381, 1977.

Heymsfield, A. J., Winker, D. and van Zadelhoff, G. J.: Extinction-ice water content-effective radius algorithms for CALIPSO, Geophys. Res. Lett., 32(10), 1–4, doi:10.1029/2005GL022742, 2005.

Mcfarquhar, G. M. and Heymsfield, A. J.: Parameterization of tropical cirrus ice crystal size distributions and implications for radiative transfer: Results from CEPEX, J. Atmos. Sci., 54(17), 2187–2200, doi:10.1175/1520-0469(1997)054<2187:POTCIC>2.0.CO;2, 1997

Page 2, L51: Fu and collaborators and Mitchell and collaborators have done some work with CALIPSO that might be relevant here, particularly for occurrence and particle size. IWC from CALIPSO is harder.

Thank you for this recommendation. We added several references (line 57 – 62): "Using satellite observations from the Cloud-Aerosol Lidar and Infrared Pathfinder Satellite Observation (CALIPSO), Mitchell et al. (2018) showed the dependence of ice particle effective diameter on temperature, latitude, season and topography. Thorsen et al. (2013) used CALIPSO data to examine cloud fraction of tropical cirrus clouds and showed dependence on altitude and diurnal cycle. Tseng and Fu (2017) used CALIPSO and Constellation Observing System for Meteorology, Ionosphere, and Climate (COSMIC) data and found that the tropical cold point

tropopause temperature is a controlling factor of cirrus cloud fraction in the tropical tropopause layer."

References added:

Mitchell, D. L., Garnier, A., Pelon, J. and Erfani, E.: CALIPSO (IIR-CALIOP) retrievals of cirrus cloud ice-particle concentrations, Atmos. Chem. Phys., 18(23), 17325–17354, doi:10.5194/acp-18-17325-2018, 2018.

Thorsen, T. J., Fu, Q., Comstock, J. M., Sivaraman, C., Vaughan, M. A., Winker, D. M., and Turner, D. D.: Macrophysical properties of tropical cirrus clouds from the CALIPSO satellite and from ground-based micropulse and Raman lidars, J. Geophys. Res. Atmos., 118, 9209–9220, doi:10.1002/jgrd.50691, 2013.

Tseng, H.-H. and Fu, Q.: Temperature control of the variability of tropical tropopause layer cirrus clouds. Journal of Geophysical Research: Atmospheres, 122, 11,062–11,075. https://doi.org/10.1002/2017JD027093, 2017.

Page 4, L107: CAM6-nudg? Typo? Seems like you are using this throughout, but I don't see it defined.

We added clarification (line 119 – 121): "Maps comparing the flight tracks of in situ observations and the collocated CAM6 nudged simulations (hereafter named "CAM6-nudg" data) are shown in Figure 1."

Page 4, L110: Are you going to test the impact of this assumption? Does CAM6 have a similar or close relationship between IWC and number/size?

For the purposes of this paper, we did not test the impact of this assumption. We added a sentence to make this clear (line 441 – 443): "The assumption of ice mass and dimension relationship from Brown and Francis (1995) may also lead to uncertainties due to various ice habits."

CAM6 does not use such relationship between IWC and size. Predicted IWC and Ni are based on a two-moment microphysics scheme (Gettelman and Morrison, 2015), thus size is predicted but not based on the same assumption as the observations.

Page 4, L113: since CAM6 has 2 moments and a distribution, wouldn't it be wise to show the size distribution from observations (not just the mean diameter) and from CAM to see if there are biases in the shape or in parts of the size distribution?

Thank you for this comment. As mentioned above, we added **Figure 4** that addresses this concern by comparing the observed size distribution with the reconstructed model size distribution both before and after applying the size constraint.

Page 4, L119: 1hz is only maybe 200m horizontal. How can that be compared with a global model at 100km resolution?

As mentioned above, we now use a new method that compares 430-s averaged observations with grid-mean quantities from simulations.

Page 4, L121: does CAM6 also use Murphy and Koop? Could that be an issue (probably not).

This is a good question, and one we should have been more clear addressing. It was noted in the original Figure 7 caption that we used the equations from Murphy and Koop (2005) for calculation of RHi in both observations and simulations. We added a clarification in section 2.2 (line 196 – 197): "Simulated RHi is calculated from simulated specific humidity and temperature, and the calculation of saturation vapor pressure with respect ice is based on the equation from Murphy and Koop (2005)."

Page 4, L123: whereas â˘A˘T> where

Revised. (line 137 – 138) "Measurements are separated by cloud condition where in-cloud condition is defined by the presence of at least one ice crystal from the Fast 2-DC probe (Ni > 0 L^{-1})."

Page 4, L128: you might note that some latitudes have some very different regimes.

We addressed this by adding a sentence in section 2.1 (line 142 – 143): "The majority of observations in the SH midlatitude and tropical regions are located over the oceans, while the observations of NH midlatitude and polar regions are predominantly over land."

Page 5, L138: I'm not sure I found where this size cutoff is noted. Is it wise to proceed with only half the size distribution? Seems like that would strongly affect how forceful you can make the conclusions. It also means the model needs to be sampled carefully.

Thank you for pointing this out. The original manuscript did mention the size cutoff in a paragraph before that sentence. This description of size restriction is now in line 127 – 128: "In order to mitigate the shattering effect, particles with diameters < 62.5 μm (i.e., first two bins) are excluded in the Fast-2DC measurements when calculating IWC, Ni and Di."

Page 5, L140: So, I assume this is then a sampling bias to your observational data set?

Yes, we added a sentence to address this (line 153 – 155): "The higher Di in this study also leads to lower range of Ni (0.01 – 1000 L^{-1}) and higher range of IWC (10^{-5} – 10 g m^{-3}) compared with that previous study (i.e., Ni from 0.1 – 10^5 L^{-1} and IWC from 10^{-7} – 1 g m^{-3}), representing the sampling bias towards larger particles in this study."

Page 5, L150: it would be also worth noting the most ice relevant adjustments in CAM6: the use of Hoose et al mixed phase ice nucleation, and Shi et al. modifications for pre-existing ice.

To address this comment, we added a sentence in section 2.2 (line 168 – 171): "The model uses Wang et al. (2014b) for ice nucleation, which implemented and improved Hoose et al. (2010) by considering the probability density function of contact angles for the classical nucleation theory. The model also uses Shi et al. (2015) for modifications of pre-existing ice."

References added:

Hoose, C., Kristjánsson, J. E., Chen, J. P. and Hazra, A.: A classical-theory-based parameterization of heterogeneous ice nucleation by mineral dust, soot, and biological particles in a global climate model, J. Atmos. Sci., 67(8), 2483–2503, doi:10.1175/2010JAS3425.1, 2010.

Wang, Y., Liu, X., Hoose, C., and Wang, B.: Different contact angle distributions for heterogeneous ice nucleation in the Community Atmospheric Model version 5, Atmos. Chem. Phys., 14, 10411–10430, https://doi.org/10.5194/acp-14-10411-2014, 2014b.

Page 6, L169: this is a pretty substantial limitation and should be noted much earlier in the text and even have caveats in the abstract. Showing model size distributions, I think is critical here. Are you calculating simulated IWC without the small particles? Would that skew the results?

We appreciate your comment, and we agree it is a limitation of this study. To address this, we added a comment on this limitation in our abstract (line 14 – 15): "Observed and simulated ice mass and number concentrations are constrained to ≥ 62.5 μm to reduce potential uncertainty from shattered ice in data collection."

As mentioned above, we added clarification of the size restriction to model output in section 2.2. A new Figure 4 is added to illustrate the particle size distributions before and after size restriction. We also added a comment on this caveat in section 4 (line 439 – 444): "It is possible that small ice crystals < 62.5 μm may have formed under high Na but are excluded due to the size constraint. … These caveats call for more investigation on small ice measurements, INP measurements at temperature ≤ -40°C, and measurements of various ice habits."

Page 6, L172: as noted above I think the method here is critical. Please describe it. I would feel more comfortable if you show he size distribution by deriving it from the mu and lambda of the gamma distributions, to understand the truncation issue.

This comment has been addressed above by revising section 2.2 and adding the new Figure 4.

Page 6, L177: I suggest that this is a major limitation of correlating Na500 with INP at the temperatures you are working with: INP activation is a strong function of temperature.

This is a valid concern. We added a sentence to the discussion section to address this as a caveat (line 440 – 441): "Additionally, because INP activation is highly dependent upon temperature, we acknowledge the limitation of using Na_{500} to indicate INP concentrations."

Page 6, L187: do you want to comment why here? SH is oceanic, NH is continental.

This is a helpful comment. We addressed this by adding this sentence (line 234 – 236): "These hemispheric differences in midlatitudes may be due to airmass differences between NH (more continental) and SH (more oceanic) and/or more anthropogenic emissions in the NH."

Page 6, L190: tropical regions with colder temps might have more small crystals. Would this affect the CAM v. OBS results? I'm concerned you have not filtered the cam results by truncating size distributions.

As noted in previous comments, after averaging observations by every 430 seconds, simulated IWC in new **Figure 5** becomes more comparable to the observations compared with our original method that compares 1-Hz observations and simulated in-cloud quantities. In new Figure 5, the tropics actually show smaller differences between simulated and observed IWC compared with those in the midlatitudes, which suggests that size restriction is not the main reason for model biases in this comparison of IWC.

Page 6, L194: I find the fact that you can get the OLR right with 10x less ice a little bit strange. Does ice mass not mater as all? Or does the di change compensate? Or the underestimation a product of the Observations really missing a lot of small ice? These don't seem to work the same way. So, I am concerned that you are comparing 1hz IWC v. 100km IWC and this is producing anomalous results.

As we mentioned above, the model biases of IWC become smaller when comparing grid-mean simulated quantities with 430-s averaged observations. We revised the text for new Figure 5 (line 247 – 251): "The CAM6-nudg data underestimate and overestimate IWC in the NH and SH by 0.5 – 1 orders of magnitude, respectively, with the largest discrepancies in the midlatitudes. The simulations overestimate Ni in the tropics and polar regions in both hemispheres by 0.5 – 1 orders of magnitude, and overestimate Ni in the southern hemispheric midlatitude by 1 – 2 orders of magnitude. The simulated Di is about half of the observed values in most regions except polar regions."

The abstract is also revised (line 16 – 18): "Comparing with averaged observations at ~100 km horizontal scale, simulations are found to underestimate (overestimate) IWC by a factor of 3–10 in the Northern (Southern) Hemisphere."

Page 7, L208: the more interesting comparison to me with Righi ET al 2020 would be how they did their comparisons between model and observations, and what sensitivity and size range did their data have? Is it the same or different than here?

Righi et al. (2020) did a comparison between 1-Hz observations and in-cloud quantities from model output. Their analysis is similar to our Figure 6 (RHi versus temperature plot), which showed the average values of RHi, Ni and Di in each temperature bin. One major difference between their study and ours is the size range of ice as they used 3 – 1280 μm. We added clarification on their method in several places.

(line 192 – 194) "Both methods have been previously used in model evaluation, such as D'Alessandro et al. (2019) which compared 200-s averaged aircraft observations with simulated

grid-mean quantities, and Righi et al. (2020) which compared 1-Hz aircraft observations with simulated in-cloud quantities."

(lines 261 – 266) "A previous study by Righi et al. (2020) evaluated the ice microphysical properties in EMAC-MADE3 aerosol–climate model (i.e., ECHAM/MESSy Atmospheric Chemistry-Modal Aerosol Dynamics model for Europe adapted for global applications, 3rd generation) by comparing in-cloud quantities from model output with 1-Hz in situ observations of multiple aircraft field campaigns from 75ºN to 25ºS (Krämer et al., 2009, 2016, 2020). Although that study included more smaller ice particles (3 – 1280 µm) compared with this study, they still showed low biases of simulated Di at 190 – 243 K, low biases of simulated IWC at 205 – 235 K, as well as high biases of simulated Ni above 225 K, ..."

Page 7, L215: is the RHI data averaged over similar ranges to the cam observations? It would seem this would be required for a reasonable comparison.

Previously, the comparison was between RHi from 1-Hz observations and CAM6. In the revised manuscript, we averaged the observations by every 430 seconds, including cloud properties and meteorological conditions (such as temperature, RHi and vertical velocity). The **new Figure 7** shows 430-s averaged RHi observations. The clarification is added in section 2.2 (line 186 – 189): "In order to examine observations and simulations on more comparable scales, a running average of 430 seconds was calculated for meteorological parameters (i.e., temperature and RHi) and microphysical properties (i.e., IWC, Ni and Di), which translates to ~100 km horizontal scales since the mean true air speed below -40°C for all campaigns was 230 m/s (supplementary Figure S2)."

Page 7, L225: it's half the scale of the CAM simulations. Also, note that CAM has a wsub minimimum value of a few cm/s, and in upper trop clear sky it's probably at that limit. One complication is that wsub comes from TKE as you note, which comes from the turbulence scheme. High wsub indicates convection and turbulence would be active, so the pathway for freezing may be very different, as active convection would create liquid that would either be homogenously frozen in the microphysics or frozen with specified size in the macro physics. It would not run through the activation code. I.e. high wsub might just indicate convective outflow. Can you check this?

This is a great comment. We added a new supplementary **Figure S5** to show the locations where model output wsub exceeds 0.5 m/s, as well as where observed vertical velocity is greater than 1 m/s for in-cloud conditions. Based on this figure, the majority of in-cloud samples do not show very high wsub or vertical velocity. We pointed out that more future work is needed to track the origin of cirrus clouds formed in both model and observations to distinguish the impacts from convection. We added this discussion in section 3.2 (line 299 – 305): "We further examine the potential impact of convection in simulations and observations. Supplementary Figure S5 shows the locations where w > 1 m/s is seen in the observations as well as where wsub > 0.5 m/s is seen in the CAM6-nudg data for in-cloud conditions. Since wsub in CAM6 is based on the turbulent scheme, higher wsub values indicate that the convection scheme may be active and produce detrained ice in convective outflows. The majority of observed and simulated in-cloud samples do not appear to have high w or wsub, indicating that detrained ice from the convection is

unlikely a significant contribution. More future investigation is needed to track cirrus cloud origins and quantify impacts from convection."

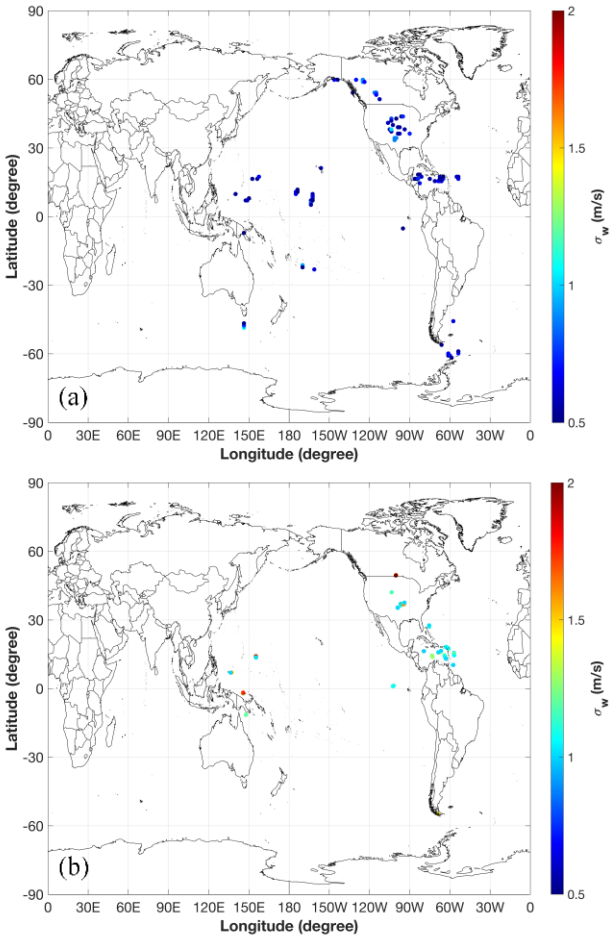

Figure S5. (a) Locations of simulated in-cloud samples with wsub > 0.5 m/s, color coded by σ_w. (b) Locations of observed in-cloud samples with vertical velocity > 1 m/s, color coded by σ_w calculated for every 430 seconds.

Page 8, L255: decrease

Changed "decreases" to "decrease".

Page 9, L262: is rhmini set to 80% in the simulations? How is ice formed? With a RH threshold? I am not sure CAM6 has such a closure. Please state the value. The Gettelman et al 2010 reference is for CAM5.

This is a good question. For the ice cloud fraction parameterization, the RHi_{min} parameter was set to 80% and RHi_{max} parameter was set to 100% in the CAM6 simulation, which are the same as CAM5. For cirrus clouds, heterogeneous nucleation can begin after reaching a minimum threshold 100%, which technically is 120% when accounting for a sub-grid variability scaling factor of 1.2 (Wang et al., 2014a). The homogeneous nucleation RHi threshold is around 150% –

160%. Beside the RHi thresholds, ice nucleation is also dependent upon additional constraints of temperature and vertical velocity (Liu et al., 2007; Liu and Penner, 2005).

We have revised our discussion of the effects of RHi on microphysical properties (line 341 – 346): "In contrast to observations, both CAM6-nudg and CAM6-free simulations show bimodal distributions of IWC and Ni with the primary peak at 100% RHi and the secondary peak at 80% RHi. The secondary peak at RHi 80% is likely produced by the RHi_{min} parameter reflecting sub-grid scale RHi variance as mentioned above (Gettelman et al., 2010), which was set at the default value (80% RHi) for both simulations. The primary peak at 100% RHi is likely a result of the minimum threshold for heterogeneous ice nucleation being set at 120% as well as a sub-grid variability scaling factor 1.2 being considered (Wang et al., 2014a)."

Page 9, L266: have you shown where in parameter space (RHI, Temp, Di, Ni) the IWC is most biased in the observations? I think it would be great to summarize this in the text. Maybe this comes later?

We added **supplementary Figure S1** and a discussion in section 2.1 (line 155– 158): "The relationships of IWC with respect to meteorological conditions (i.e., temperature and RHi) and other microphysical properties (i.e., Ni and Di) are shown in supplementary Figure S1. The distributions of IWC samples are relatively uniform at various temperature and RHi, while more IWC samples are correlated with Di between 100 and 300 µm."

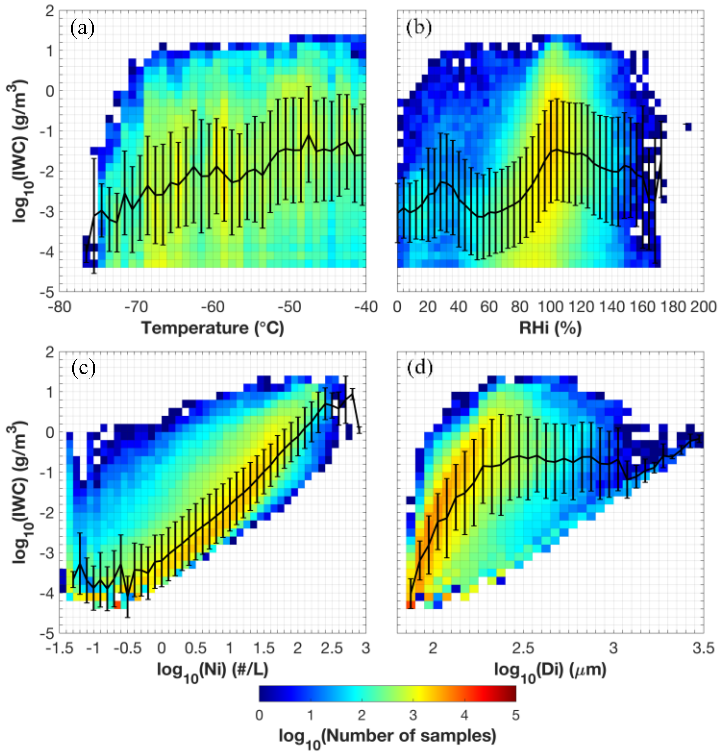

Figure S1. Number of samples of log-scale IWC values in the observations related to various meteorological conditions (i.e., (a) temperature and (b) RHi) and microphysical properties (i.e., (c) log-scale Ni and (d) Di). Average IWC values and standard deviations are represented by black lines and whiskers, respectively. Note that all samples are for temperature ≤ -40ºC.

Page 9, L269: this gets back to sampling. And remember the model represents a distribution, which you should plot, I think. There is variability in a single value in the model. It's not one value.

We added the particle size distribution in new Figure 4.

Page 9, L278: see above. The ice formation mechanism in CAM might not be what you think in the presence of convection at cirrus temps.

We agree and added supplementary Figure S5 as discussed above.

Page 9, L281: I do not think using cloud fraction here is wise. Cloud fraction is a function of scale as well as the detection threshold: if the OBS don't see any Di < 65um, that will skew things itself relative to CAM. Maybe you should use something easier to make consistent between model and OBS. I'm not sure what that is, maybe Ni since it is an in cloud only quantity. Also, can you sample aerosols in cloud in the Obs? If not, then are you filtering that out of the model?

We would like to clarify that the cloud fraction plotted in the original Figure 13 and the new Figures 15 and 16 is not the "Cloud Fraction" variable from the model output. The cloud fraction for simulation in these figures is calculated using the number of in-cloud conditions defined by the concurring IWC and Ni values greater than certain thresholds, and normalized by the total number of samples in each temperature – Na bin. Therefore, the definition of cloud fraction in our study actually follows the reviewer's suggestion of using Ni since it is an in-cloud only quantity. This is clarified in section 4.3 (line 382 – 384): "Cloud fraction is calculated in each temperature – Na bin by normalizing the number of in-cloud samples with the total number of samples in that bin for both observations and simulations." The in-cloud condition for simulation is defined here (line 209 – 211): "In-cloud conditions in simulations are defined by concurring conditions of IWC > 10^{-7} g m^{-3} and Ni > 10^{-4} L^{-1} based on size-restricted grid-mean quantities. These thresholds are the lower limits from observations after calculating the 430-s averages." And to answer your question of aerosol sampling in clouds, yes, the aerosol measurements are available for in-cloud conditions.

Page 10, L300: it's not clear to me there was much shown with the CAM6 free running simulations. I assume you will summarize Any differences later in this section?

See our previous responses regarding differences between CAM6-nudg and CAM6-free.

Page 10, L304: since zonal locations in each latitude band are narrow, are you sure this is general and not just a land-sea contrast? Is it anthropogenic aerosols or just land v. ocean?

We agree that both land-sea contrast and anthropogenic aerosols are possible reasons for the hemispheric differences. We acknowledge the possibility of both reasons in our revised text (line 410 – 412): "The hemispheric differences between NH and SH midlatitudes indicate a possible role of anthropogenic aerosols and/or land-sea contrast in controlling ice microphysical properties."

Page 11, L325: could the model just be producing smaller crystals that are not seen in the observations when Na100 is large?

This is a good question. It is possible that small ice crystals may have formed at high Na_{500} and Na_{100} and have been cut out due to size restriction. We added a clarifying sentence to address this (line 439 – 440): "It is possible that small ice crystals < 62.5 μm may have formed under high Na but are excluded due to the size constraint."

Page 11, L330: this statement is a bit to grandiose: it's not really comprehensive and there are a limited set of factors.

We deleted the word "comprehensive" in that sentence.

Page 11, L331: some more summary of what the results actually said here is warranted. What did you discover about geographical locations? Also, I'm not sure zonal averages are that helpful if the mix regimes, as noted earlier.

We addressed this comment by adding more summary on regional variations in section 5 (line 450 – 454): "For both observations and simulations, higher ice supersaturations and stronger vertical motions are shown in tropical and midlatitude regions, which possibly lead to increased homogeneous nucleation and convection-generated cirrus, consistent with higher IWC and Ni and lower Di in these regions compared with polar regions. In addition, underestimating aerosol indirect effects in the simulations likely contributes to the underestimation of IWC in the NH."

Page 11, L332: I'm still not sure the comparisons and elimination from the model of small ice are done correctly.

See previous comments on model size truncation to remove ice particles smaller than 62.5 μm.

Page 25, L592: I would recommend collapsing this to put the observations (maybe as a shaded region) on the same plot as the simulations. It makes comparisons easier and results in fewer figure panels.

We thank you for this recommendation. The original Figure 4 has been moved to supplementary material. The new **Figure 5** now shows both model and observation in each sub-panel for convenience.

Page 28, L610: Figures 6 and 7: maybe you could normalize these to get them on the same scale. What is going on in CAM with regular frequency peaks in temperature?

We have adjusted the color scales for **Figures 6 – 10** so that they are the same. To answer your question on the regular frequency peaks in temperature in the simulations (**new Figure 8**), we attribute this discontinuity in temperature to larger distances between model vertical levels in the upper troposphere over the tropics. We added this clarification (line 287 – 288): "Note that the simulation samples in the tropical regions show peak frequencies at certain temperatures due to larger bin sizes of pressure levels in the lower latitudes."

Response to the Reviewer 2's comments:

Anonymous Referee #2

This paper represents a nice study of microphysical observations versus climate modeling. The paper is well written and clear. I shear some of the same concerns as the other reviewer "Andrew Gettelman" but I think this paper could be published after all comments are addressed. Below are my main comments and concerns.

Line 65: Is the reason for increased crystal size with increased aerosols due to the competition between homogeneous and heterogeneous ice nucleation and that you actually have fewer ice crystal concentration in the polluted environment?

Great question. Based on the Chylek et al. (2006) study, they speculate that in the polluted environment, more ice nuclei form ice particles via heterogeneous nucleation, therefore reducing the amount of excess water vapor over ice saturation and making homogeneous nucleation a more difficult pathway. We added this clarification (line 79 – 83): "Chylek et al. (2006) showed an increase in ice crystal size during the more polluted winter months compared with cleaner summer months over the eastern Indian Ocean, which the authors speculate to be due to heterogeneous nucleation occurring at lower ice supersaturation compared with homogeneous nucleation, therefore reducing the ambient ice supersaturation magnitude and making homogeneous nucleation a more difficult pathway."

Line 73: How does the increase in aerosol number concentration help increase the size of ice crystals?

This is an excellent question, and one we also asked ourselves. In a closed system with limited water vapor supply, one would expect ice crystal number concentration (Ni) and mean diameter (Di) to be anti-correlated, similar to the conventional Twomey effect. In our analysis of the in-situ observations, cirrus clouds may have experienced more complex ambient conditions. One possible scenario is that cirrus clouds from in-situ observations could have experienced a series of different magnitudes of ice supersaturation in their evolution history. This could have induced several ice nucleation events, forming new ice particles in addition to the preexisting ice particles. As a result, Ni would increase, and Di would also increase due to the growth of the previously formed ice particles. Previous observation-based studies on cirrus cloud evolutionary trend (Diao et al., 2013, 2014) support the increase of both Ni and Di during cirrus evolution. In the study of Diao et al. (2013), we found that as cirrus clouds evolve from nucleation phase to early growth and later growth phases, both Ni and Di increase.

References mentioned above:

Diao, M., Zondlo, M. A., Heymsfield, A. J., Beaton, S. P. and Rogers, D. C.: Evolution of ice crystal regions on the microscale based on in situ observations, Geophys. Res. Lett., 40(13), 3473–3478, doi:10.1002/grl.50665, 2013.

Diao, M., Zondlo, M. A., Heymsfield, A. J. and Beaton, S. P.: Hemispheric comparison of cirrus cloud evolution using in situ measurements in HIAPER Pole-to-Pole Observations, Geophys. Res. Lett., 41(11), 1–8, doi:10.1002/2014GL059873, 2014.

Line 86: I suggest to rephrase: ": : :.and found a decrease in Ni with increasing aerosol concentration due to the : : :: : :"

We revised this sentence (line 98 – 100): "Shi et al. (2015) added the effects of pre-existing ice into the Community Atmosphere Model Version 5 (CAM5) and found a decrease in Ni with increasing aerosol concentration due to the reduction of homogeneous nucleation frequency."

Line 131-133: Are there differences between ocean and land as well?

This is a good question. Based on the map of flight campaigns (their Figure 1) from Krämer et al. (2020), our dataset has more sampling over the ocean compared with theirs, especially for sampling over the Pacific Ocean from the HIPPO Global campaign.

Line 148: If you used the microphysical version including graupel and hail (MG3) you should cite Gettelman et al 2019, "The impact of rimed ice on Global and Regional Climate" in JAMES

For the simulations in this paper, we used the MG2 microphysics scheme. As you noted, this does not include graupel and hail. Therefore we revised that sentence (line 164 – 166): "An improved bulk two-moment cloud microphysics scheme has been implemented (Gettelman and Morrison, 2015) that replaces diagnostic treatment of rain and snow with prognostic treatment of all hydrometeors (i.e., rain and snow)."

Line 154. Do the nudged runs also use prescribed sea-surface temperature?

Yes. The details are described in section 2.2 (line 175 – 176): "All simulations are conducted using prescribed sea-surface temperature and present-day aerosol emissions and include a 6-month spin-up time."

Line 166: If you disregard the smallest sizes in the observations to define in-cloud conditions, but account for all sizes in the model when defining in-cloud conditions how often do you miss observed in-cloud conditions compared to modeled in-cloud conditions?

This is a good question. We use **supplementary Figure S6** to contrast with Figure 12 for the impact of including small ice particles in the simulations. Figure S6 is similar to Figure 12, except for using ice crystals > 1 μm in the analysis for simulated in-cloud data. Figure S6 shows a 4% increase of number of samples for simulated in-cloud conditions compared with Figure 12 (restricted to ≥ 62.5 μm) (line 318 – 320): "When using a lower size cut-off (1 μm) of ice particles for the simulation data, the number of in-cloud samples increases by 4% (supplementary Figure S6)."

Line 167: Why is the additional constraint on cloud fraction not used for the CAM-nudged?

We appreciate your question, and we should have clarified. This constraint was indeed used on both CAM6 simulations. We reworded this sentence to be clearer (line 213 – 214): "An additional constraint on cloud fraction > 10^{-5} was applied to both nudged and free-running simulations to exclude extremely low values."

Line 181: When mentioning figure 4 I suggest adding a sentence stating that 3 top rows are observations and 3 lower rows are model. Perhaps you can add a label in the figure as well.

Thank you for this recommendation. Since both reviewers mentioned the difficulty with this figure, the new **Figure 5**, now includes both observations and simulations in each sub-panel.

Line 187: Mention that the CAM6-nudg data is the 3 bottom rows

We appreciate your recommendation. As we mentioned above, the new Figure 5 now includes both observations and simulations in each sub-panel.

Line 207: Did you include the pre-existing ice option by Shi et al in the simulations? Perhaps you should mention that here.

Yes, the model did include the effects of pre-existing ice from Shi et al. (2015). We added this clarification in the methods section (line 170 – 171): "The model also uses Shi et al. (2015) for modifications of pre-existing ice."

Line 210: I suggest using same color scale between figure 6 and figure 7

Figures 6 – 11 are revised to use the same color scale.

Line 211: What is the cause of the systematic "wave" showing up in the tropical RHi in Figure 7?

This is a good question. We added an explanation of this feature (line 287 – 288): "Note that the simulation samples in the tropical regions show peak frequencies at certain temperatures due to larger bin sizes of pressure levels in the lower latitudes."

Line 212: It is difficult to see the difference between the solid line and the dashed line in figures 6 and 7.

We addressed this issue by making both lines thicker.

Line 224: Figure 8 and 9 (and other figures with variance of w). Since this value is never negative, I suggest starting the scale at zero.

Thank you for this recommendation. We changed the ordinate range to start from zero for **Figures 9 to 11**.

Line 224. The 200 seconds of data corresponding to 46 km, is that true for all flights?

The mean true air speed of ~230 m/s was calculated based on the entire dataset of seven campaigns for all temperatures ≤ -40°C. We added supplementary **Figure S2** to show the mean true air speed at various temperatures averaged for the entire dataset. For each flight, the mean true air speed in the upper troposphere is around this value.

Line 252: Figure 11: Are the number of samples normalized for the colorbar? I also suggest label the top row as observations, middle as CAM6-nudg and bottom as CAM6-free data.

The original figure 11 was not normalized, and the color code shows the exact number of samples in each bin. We added labels for each row in the new **Figures 12 – 14**, to distinguish between different datasets.

Line 273: Figure 12. I do not see a large positive correlation between Di and w. I would suggest state: ": : :..which differs from the slight observed positive: : :.." Figure 13. Label the two left columns as Na500 and the two right columns as Na100. In the caption, figures q-t are not described.

Thank you for this recommendation. We revise this sentence (line 363 – 364): "This slight positive Di - σ_w correlation is likely due to the growth of ice particles as cirrus clouds evolve with continuous updrafts that supply excess water vapor above ice saturation, ..."

We separated the original Figure 13 into the new **Figures 15 and 16** for Na_{500} and Na_{100}, respectively. We added description to the last row in Figure 15 caption.

Effects of Thermodynamics, Dynamics and Aerosols on Cirrus Clouds Based on In Situ Observations and NCAR CAM6 Model

Ryan Patnaude[1], Minghui Diao[1], Xiaohong Liu[2], Suqian Chu[3]

[1]Department of Meteorology and Climate Science, San Jose State University, San Jose, 95192, USA
[2]Department of Atmospheric Sciences, Texas A&M University, College Station, 77843, USA,
[3]Department of Atmospheric Science, University of Wyoming, Laramie, 82071, USA

Correspondence to: Minghui Diao (minghui.diao@sjsu.edu)

Abstract. Cirrus cloud radiative effects are largely affected by ice microphysical properties, including ice water content (IWC), ice crystal number concentration (Ni) and mean diameter (Di). These characteristics vary significantly due to thermodynamic, dynamical and aerosol conditions. In this work, a global-scale observation dataset is used to examine regional variations of cirrus cloud microphysical properties, as well as several key controlling factors, i.e., temperature, relative humidity with respect to ice (RHi), vertical velocity (w), and aerosol number concentrations (Na). Results are compared with simulations from the National Center for Atmospheric Research (NCAR) Community Atmosphere Model version 6 (CAM6). Observed and simulated ice mass and number concentrations are constrained to ≥ 62.5 μm to reduce potential uncertainty from shattered ice in data collection. The differences between simulations and observations are found to vary with latitude and temperature. ~~Specifically~~Comparing with averaged observations at ~100 km horizontal scale, simulations are found to underestimate (overestimate) IWC by a factor of ~~5–30~~ 3–10 in ~~all regions~~the Northern (Southern) Hemisphere. Simulated Ni is overestimated in most regions except Northern Hemisphere midlatitude ~~and polar regions~~. Simulated Di is underestimated by a factor of 2, especially for warmer conditions (-50ºC to -40ºC) ~~and higher Na~~, possibly due to misrepresenting ~~less effective~~ ice particle growth/sedimentation ~~and weaker aerosol indirect effects, respectively~~. For RHi effects, the frequency and magnitude of ice supersaturation is underestimated in simulations for clear-sky conditions~~., and t~~ The simulated IWC and Ni show bimodal distributions with maximum values at 100% and 80% RHi, differing from the unimodal distributions that peak at ~~instead of~~ 10~~1~~0% in the observations~~as observed~~. For w effects, both observations and simulations show variances of w (σ_w) decreasing from tropics to polar regions, but simulations show much higher σ_w for in-cloud condition than clear-sky condition. Compared with observations, simulations show weaker aerosol indirect effects with smaller increase of IWC and Di at higher Na. These findings provide an observation-based guideline for improving simulated ice microphysical properties and their relationships with key controlling factors at various geographical locations.

1 Introduction

Cirrus clouds represent one of the most ubiquitous cloud types with an estimated global coverage of approximately 20% to 40% (Mace and Wrenn, 2013; Sassen et al., 2008). According to the fifth assessment of the United Nations

Intergovernmental Panel on Climate Change (IPCC) report (Boucher et al., 2013), the largest uncertainty in estimating future climate change stems from clouds and aerosols. Unlike most other cloud types, cirrus clouds may produce a net positive or negative radiative forcing depending on their microphysical properties (Stephens and Webster, 1981; Zhang et al., 1999), which are affected by meteorological conditions and aerosol distributions. Tan et al. (2016) showed that the radiative effects of misrepresenting the prerequisite condition of cirrus clouds – ice supersaturation (ISS, where relative humidity with respect to ice (RHi) > 100%) – can lead to an average bias of +2.49 W/m^2 at the top of the atmosphere. Other modelling studies found large differences in the net cloud radiative forcing depending on the fraction of activated ice nucleating particles (INPs) and the nucleation mechanisms (i.e., homogeneous and heterogeneous nucleation) through which the clouds form (Liu et al., 2012; Storelvmo and Herger, 2014). The large uncertainties in cirrus cloud radiative forcing illustrate the need for further study on cirrus cloud microphysical properties as well as their controlling factors in various geographical locations.

Ideally, a comprehensive quantification of cirrus cloud microphysical properties globally based on high-resolution, in situ observations would mitigate many uncertainties. However, challenges remain in field measurements to achieve such spatial coverage. Previously, efforts have been made to understand cirrus cloud properties based on their geographical locations. Diao et al. (2014b) performed a hemispheric comparison of in situ cirrus evolution and found little difference in the clear-sky ISS frequency as well as the proportion of each evolution phase between the Northern and Southern Hemispheres (NH and SH, respectively). In situ observations of tropical, midlatitude, and polar cirrus clouds have shown that IWC can vary orders of magnitude depending on the geographical locations (Heymsfield, 1977; Heymsfield et al., 2005, 2017; Mcfarquhar and Heymsfield, 1997; Schiller et al., 2008). ~~Another study investigated the ice water content (IWC) and snowfall rates for tropical, midlatitude, and Arctic cirrus clouds using in situ observations and found a geographical dependence of IWC.~~ Wolf et al. (2018) used balloon-based in situ observations to analyze microphysical properties of Arctic ice clouds and found differences in particle size distributions (PSDs) depending on the cloud origin. Krämer et al. (2016, 2020) developed a cirrus cloud climatology, focusing on tropical and midlatitude cirrus clouds, and showed that cloud thickness is larger at lower altitudes, and thus producing a more negative radiative forcing. Moving from north to south using lidar-based observations from two research cruises starting from Leipzig, Germany, one to Punta Arenas, Chile and the other one to Stellenbosch, South Africa, Kanitz et al. (2011) observed a decrease in the efficiency of heterogeneous nucleation in the SH, which could be a result of fewer INPs. This hemispheric difference in aerosol indirect effects is consistent with significantly higher aerosol number concentrations in the NH (Minikin et al., 2003). Using satellite observations from the Cloud-Aerosol Lidar and Infrared Pathfinder Satellite Observation (CALIPSO), Mitchell et al. (2018) showed the dependence of ice particle effective diameter on temperature, latitude, season and topography. Thorsen et al. (2013) used CALIPSO data to examine cloud fraction of tropical cirrus clouds and showed dependence on altitude and diurnal cycle. Tseng and Fu (2017) used CALIPSO and Constellation Observing System for Meteorology, Ionosphere, and Climate (COSMIC) data and found that the tropical cold point tropopause temperature is a controlling factor of cirrus cloud fraction in the tropical tropopause layer.

Regional and hemispheric variations of cirrus microphysical properties are produced by various controlling factors, such as thermodynamics (i.e., temperature and RHi), dynamics (e.g., vertical velocity) and aerosols (e.g., number concentration and

composition). The effects of temperature have been extensively studied from in situ observations (Heymsfield et al., 2017; Luebke et al., 2013, 2016; Schiller et al., 2008), showing an increase of IWC towards warmer temperatures. A number of studies focused on distributions of RHi have found that in-cloud RHi occurs most frequently at or near 100% (Jensen et al., 2001; Krämer et al., 2009). Another study by Diao et al. (2017) found that using different RHi thresholds (e.g., 108% to 130%) for ice nucleation in simulations can influence IWC and ice crystal number concentrations (Ni) in convective cirrus. In addition, the spatial scales of ice supersaturated regions can vary from the micro- to mesoscales, largely depending on the spatial variability of water vapor (Diao et al., 2014a). The distributions of vertical velocity have been investigated in different types of cirrus clouds, such as in ridge-crest cirrus, frontal cirrus and anvil cirrus (Muhlbauer et al., 2014a, 2014b). Stronger updrafts are found to be associated with higher occurrence frequency of ISS inside anvil and convective cirrus (D'Alessandro et al., 2017). Regarding the effects of aerosols, Cziczo et al. (2013) and Cziczo and Froyd (2014) investigated ice crystal residuals from in situ observations and discovered that the majority of midlatitude cirrus clouds form via heterogeneous nucleation on mineral dust and metallic particles. Anthropogenic aerosols, such as secondary organic aerosols, were found to be less effective INPs compared with mineral dust (Prenni et al., 2009). Based on remote sensing data, Zhao et al. (2018, 2019) showed that the correlations between ice crystal sizes and aerosol optical depth can be either positive or negative depending on the meteorological conditions in convective clouds. Chylek et al. (2006) showed an increase in ice crystal size during the more polluted winter months compared with cleaner summer months over the eastern Indian Ocean, which the authors speculate to be due to heterogeneous nucleation occurring at lower ice supersaturation compared with homogeneous nucleation, therefore reducing the ambient ice supersaturation magnitude and making homogeneous nucleation a more difficult pathway. Using a global-scale dataset of multiple flight campaigns, Patnaude and Diao (2020) isolated individual effects on cirrus clouds from temperature, RHi, vertical velocity (w) and aerosol number concentrations (Na). They found that when Na is 3 – 10 times higher than average conditions, it shows strong positive correlations with cirrus microphysical properties such as IWC, Ni and number-weighted mean diameter (Di). These aerosol indirect effects are also susceptible to whether or not thermodynamic and dynamical conditions are controlled, demonstrating the importance of conducting a comprehensive analysis of various key controlling factors altogether.

More recently, in situ observations have been used to evaluate and improve cirrus cloud parameterizations in global climate models (GCMs). Two types of simulations have been frequently used for model evaluation, i.e., free-running (Eidhammer et al., 2014, 2017; Wang and Penner, 2010; Zhang et al., 2013) and nudged (D'Alessandro et al., 2019; Kooperman et al., 2012; Wu et al., 2017) simulations. For free-running simulations, a comparison on statistical distributions of ice microphysical properties is often used for model validation (e.g., Penner et al., 2009). The nudged simulation would nudge certain meteorological conditions towards reanalysis data, such as horizontal wind and temperature (e.g., D'Alessandro et al., 2019; Wu et al., 2017). These nudged simulations can also be output to similar location and time as those of the aircraft observations. Given the importance and limited understanding of how aerosols interact with cirrus clouds, much attention has been dedicated to the parameterization of aerosol indirect effects (Kärcher and Lohmann, 2002, 2003; Kuebbeler et al., 2014; Wang et al., 2014a). Shi et al. (2015) added the effects of pre-existing ice into the Community Atmosphere Model

Version 5 (CAM5) and found a decrease in Ni with increasing aerosol concentration due to the reduction of homogeneous nucleation frequency. Other studies also investigated the effect of updraft velocity on simulated Ni and aerosol indirect effects (Zhou et al., 2016; Penner et al., 2018).

This study aims to bridge the knowledge gap on how cirrus clouds vary depending on geographical locations and environmental conditions by using a comprehensive in situ observation dataset that includes seven U.S. National Science Foundation (NSF) flight campaigns. Observations were collected onboard the NSF/National Center for Atmospheric Research (NCAR) Gulfstream-V (G-V) research aircraft. Descriptions of the seven flight campaigns, instrumentations, model configurations of the NCAR Community Atmosphere Model version 6 (CAM6) are provided in Section 2. Both observations and simulations are used to examine the regional variations in the statistical distributions of cirrus microphysical properties, including IWC, Ni and Di (Section 3). Impacts of several key controlling factors, i.e., temperature, RHi, w and Na, are examined in Section 4. Discussions on observation-based findings and model evaluation results are included in Section 5.

2 Data and Methods

2.1 In situ observations and instrumentations

In this study, in situ airborne observations at 1 Hz are provided by instruments onboard the NSF High-Performance Instrumented Airborne Platform for Environmental Research (HIAPER) G-V research aircraft. A comprehensive global dataset is compiled based on seven major flight campaigns funded by the NSF, including START08 (Pan et al., 2010), HIPPO deployments 2–5 (Wofsy et al., 2011), PREDICT (Montgomery et al., 2012), TORERO (Volkamer et al., 2015), DC3 (Barth et al., 2015), CONTRAST (Pan et al., 2017), and ORCAS (Stephens et al., 2018). Table 1 provides a detailed summary of the seven flight campaigns, including location, duration of flights, total flight hours of all temperatures, and flight hours for in-cloud and clear-sky conditions at temperatures ≤ -40ºC only. Maps comparing the flight tracks of in situ observations and the collocated CAM6 -nudged simulations ~~data~~ (hereafter named "CAM6-nudg" data) are shown in Figure 1.

For this study, ice particle measurements are provided by the Fast 2-Dimensional Cloud particle imaging probe (Fast-2DC) with a 64-diode laser array for a range of 25 μm – 1600 μm. Larger particles can be reconstructed up to 3200 μm. The mass-Dimensional relationship of Brown and Francis (1995) is used to calculate IWC for the Fast-2DC probe, which was previously used in other studies of the Fast-2DC probe onboard the NSF G-V aircraft (Diao et al., 2014a, 2014b, 2015). Number-weighted mean diameter (Di) is calculated by summing up the size of particles in each bin using the bin center, and then dividing it by the total number of particles. In order to mitigate the shattering effect, particles with diameters < 62.5 μm (i.e., first two bins) are excluded in the Fast-2DC measurements when calculating IWC, Ni and Di. The Rosemount temperature probe was used for temperature measurements, which has an accuracy and precision of ~ ±0.3 K and 0.01 K,

respectively. All analyses are restricted to temperatures ≤ -40°C, in order to exclude the presence of supercooled liquid droplets in this study. Laboratory calibrated and quality-controlled water vapor data were collected using the Vertical Cavity Surface Emitting Laser (VCSEL) hygrometer (Zondlo et al., 2010), with an accuracy of ~6% and precision of ≤ 1%. Both temperature and water vapor are used at 1-Hz resolution for this analysis. Aerosol measurements were collected from the Ultra-High Sensitivity Aerosol Spectrometer (UHSAS), which uses 100 logarithmically spaced bins ranging from 0.06 – 1 μm. RHi is calculated using saturation vapor pressure with respect to ice from Murphy and Koop (2005). The combined RHi uncertainties from the measurements of temperature and water vapor range from 6.9% at -40ºC to 7.8% at -78ºC. Measurements are separated by cloud condition where~~as~~ in-cloud condition is defined by the presence of at least one ice crystal from the Fast 2-DC probe (Ni > 0 L^{-1}). The same in-cloud definition has been used by several previous studies (D'Alessandro et al., 2017; Diao et al., 2014a, 2014b, 2015, 2017; Tan et al., 2016), and all other samples are defined as clear sky. For regional variation analysis, data are binned by six latitudinal regions in the two hemispheres, that is, NH polar (60ºN – 90ºN), SH polar (60ºS – 90ºS), NH midlatitude (30ºN – 60ºN), SH midlatitude (30ºS – 60ºS), NH tropics (0º – 30ºN), and SH tropics (0º – 30ºS). The majority of observations in the SH midlatitude and tropical regions are located over the oceans, while the observations of NH midlatitude and polar regions are predominantly over land.

The vertical profiles of observed in-cloud temperature, clear-sky potential temperature (Θ), and their correlations are shown in Figure 2. The observations sampled temperatures from -78ºC to -40ºC and altitudes from 5 – 15 km, while a previous study of Krämer et al. (2020) sampled -91ºC to -30ºC and 5 – 19 km (their Figure 2). The lowest temperatures are found in the tropical regions and at the highest altitudes, whereas polar regions show more observations at lower altitudes that satisfy temperature ≤ -40ºC. Distributions of cirrus cloud properties (i.e., IWC, Ni, Di), in-cloud and clear-sky RHi, and clear-sky water vapor mixing ratio for the observation dataset are shown in Figure 3. Di increases with decreasing altitudes, IWC slightly increases with decreasing altitudes, and Ni is almost independent of altitudes. Clear-sky RHi and water vapor mixing ratio both increase with decreasing altitudes, while in-cloud RHi is centered around 100% and shows smaller dependency on altitudes. Compared with Figure 3 in Krämer et al. (2020), 48% of their ice particle samples have Di < 40 μm, which is below the size cut-off used in this study. The higher Di in this study also leads to lower range of Ni (0.01 – 1000 L^{-1}) and higher range of IWC (10^{-5} – 10 g m^{-3}) compared with that previous study (i.e., Ni from 0.1 – 10^5 L^{-1} and IWC from 10^{-7} – 1 g m^{-3}), representing the sampling bias towards larger particles in this study. The relationships of IWC with respect to meteorological conditions (i.e., temperature and RHi) and other microphysical properties (i.e., Ni and Di) are shown in supplementary Figure S1. The distributions of IWC samples are relatively uniform at various temperature and RHi, while more IWC samples are correlated with Di between 100 and 300 μm.

2.2 Climate model description and experiment design

This study uses model simulations based on the NCAR CAM6 model. Compared with its previous version – the CAM5 model, CAM6 implemented a new scheme, the Clouds Layers Unified by Binomials (CLUBB) for representations of boundary layer turbulence, shallow convection and cloud macrophysics (Bogenschutz et al., 2013). CLUBB is a higher-order

turbulence closure scheme that calculates prognostic higher-moments based on joint probability density function (PDFs) for vertical velocity, temperature, and moisture (Golaz et al., 2002). An improved bulk two-moment cloud microphysics scheme has been implemented (Gettelman and Morrison, 2015) that replaces diagnostic treatment of rain and snow with prognostic treatment of all hydrometeors (i.e., rain and~~,~~ snow~~, graupel, hail~~). This is coupled with a 4-mode aerosol model (MAM4) (Liu et al., 2016) for simulations of aerosols and aerosol-cloud interactions. It allows ice crystals to form via homogeneous freezing of sulfate aerosols and heterogeneous nucleation of dust particles (Liu et al., 2007; Liu and Penner, 2005). The model uses Wang et al. (2014b) for ice nucleation, which implemented and improved Hoose et al. (2010) by considering the probability density function of contact angles for the classical nucleation theory. The model also uses Shi et al. (2015) for modifications of pre-existing ice. Finally, the deep convection scheme (Zhang and McFarlane, 1995) has been tuned to include sensitivity to convection inhibition.

Results from in situ observations are compared with two types of CAM6 simulations, nudged and free-running simulations. Simulations are based on a finite-volume dynamical core (Lin, 2004) with a horizontal resolution of 0.9º×1.25º and 32 vertical levels. All simulations are conducted using prescribed sea-surface temperature and present-day aerosol emissions and include a 6-month spin-up time. CAM6 nudged simulations are nudged spatially and temporally with meteorological data (i.e., 2-D horizontal wind and temperature) from the Modern-Era Retrospective Analysis for Research and Applications version 2 (MERRA2) (Gelaro et al., 2017), and collocated with aircraft flight tracks in space and time. A nudged simulation was conducted for each campaign independently and was combined into one data set ~~(hereafter named "CAM6-nudg")~~ to compare with observations. One free-running simulation was conducted for the duration of all flight campaigns from July 2008 to February 2016. To reduce the size of model output when comparing with observations, a total of 24 instantaneous output from the free-running simulation are combined into one data set ("CAM6-free" hereafter), which includes 00 and 12 UTC for the first day of each month in 2010. Additional sensitivity tests on different model output from the free-running simulation show very minor differences in the statistical distributions of cirrus microphysical properties and the correlations with their controlling factors when selecting different years, seasons, and days in a month.

In order to examine observations and simulations on more comparable scales, a running average of 430 seconds was calculated for meteorological parameters (i.e., temperature and RHi) and microphysical properties (i.e., IWC, Ni and Di), which translates to ~100 km horizontal scales since the mean true air speed below -40°C for all campaigns was 230 m/s (supplementary Figure S2). Grid-mean quantities from model output are used in comparisons with observations, including "IWC", "NUMICE", "QSNOW" and "NSNOW", which are mass and number concentrations of ice particles and snow, respectively. Another type of comparison between 1-Hz observations and in-cloud quantities from model output is shown in the supplementary material. Both methods have been previously used in model evaluation, such as D'Alessandro et al. (2019) which compared 200-s averaged aircraft observations with simulated grid-mean quantities, and Righi et al. (2020) which compared 1-Hz aircraft observations with simulated in-cloud quantities.

A summary of the ranges of meteorological conditions and ice microphysical properties for in situ observations and simulations is shown in Table 2. Simulated RHi is calculated from simulated specific humidity and temperature, and the

calculation of saturation vapor pressure with respect ice is based on the equation from Murphy and Koop (2005). ~~In-cloud conditions in simulations are defined by concurring conditions of IWC > 10^{-5} g m^{-3} and Ni > 10^{-2} L^{-1}, which are the lower limits from observations. In addition, analysis of simulated cirrus clouds is restricted to similar pressure ranges as those measured in the seven campaigns. An additional constraint on cloud fraction > 10^{-5} was applied to CAM6-free to exclude extremely low values. A summary of the ranges of meteorological conditions and ice microphysical properties for in situ and simulation data is shown in Table 2.~~ Simulated ice and snow are restricted to ≥~~>~~ 62.5 μm based on the size cut-off of the Fast-2DC probe by applying methods from Eidhammer et al. (2014). Based on their equations 1 to 5, we followed their assumption that the shape parameter μ equals 0 when calculating the slope parameter λ. Mass and number concentrations of ice and snow are further calculated based on integrals of incomplete gamma functions from 62.5 μm to infinity. The simulated values of IWC, Ni and Di are calculated based on the combined ice and snow population after applying the size restriction. ~~Note that due to the ice crystal size constraint, some thin cirrus may not be detected. IWC, Ni and Di values are re-calculated by combining snow and ice for their mass and number concentrations based on a similar method from , which also combined snow and ice to compare with in situ data.~~ In-cloud conditions in simulations are defined by concurring conditions of IWC > 10^{-7} g m^{-3} and Ni > 10^{-4} L^{-1} based on size-restricted grid-mean quantities. These thresholds are the lower limits from observations after calculating the 430-s averages. Note that due to the ice crystal size constraint, some thin cirrus may not be detected. In addition, analysis of simulated cirrus clouds is restricted to similar pressure ranges as those measured in the seven campaigns. An additional constraint on cloud fraction > 10^{-5} was applied to both nudged and free-running simulations to exclude extremely low values.

To visualize the impact of the size truncation on simulated data, we employed methods similar to Gettelman et al. (2020) and reconstructed the simulated particle size distributions for snow and ice in Figure 4, using gamma functions from Morrison and Gettelman (2008). Note that prior to restricting the diameters of ice and snow particles to ≥ 62.5 μm, the number density for combined ice and snow is overestimated for smaller particles (< 1000 μm) and underestimated for larger particles (≥ 1000 μm). After applying size restriction, the simulated size distribution for combined ice and snow (dashed purple line) becomes more similar to observations due to the reduction of number density of small particles.

~~In addition~~Finally, simulated aerosols number concentrations are further categorized by diameters > 500 nm and > 100 nm (i.e., Na_{500} and Na_{100}, respectively), by summing the size-restricted concentrations of the Aitken, accumulation and coarse aerosol modes. Previously, field experiments found that Na_{500} correlates well with INP number concentrations (DeMott et al., 2010). Even though that correlation was only determined based on observations warmer than -36ºC, the separation of Na_{500} and Na_{100} can help to examine the effects of larger and smaller aerosols in this work.

3 Regional variations of cirrus cloud characteristics

3.1 Cirrus cloud microphysical properties with respect to temperature

Three cirrus cloud microphysical properties, IWC, Ni and Di are examined in relation to temperature at six latitudinal regions (Figure 5~~4~~), the standard deviations of the IWC, Ni and Di in each temperature bin are shown in supplementary Figure S3. The 1-Hz observations of IWC and Ni in the NH indicate clear latitudinal differences with the highest values occurring in the midlatitudes, followed by tropics, then polar regions for temperatures between -40ºC and -60ºC, while for colder temperatures the NH tropical region shows the highest IWC. In the SH, the highest IWC and Ni occur in the tropics, followed by the polar regions and midlatitudes. Comparing the two hemispheres, IWC and Ni show significant reductions by ~1 order of magnitude from NH midlatitude to SH midlatitude (Figure 5 b, e). These hemispheric differences in midlatitudes may be due to airmass differences between NH (more continental) and SH (more oceanic) and/or more anthropogenic emissions in the NH. The IWC, Ni and Di are relatively similar between NH and SH tropical regions, while IWC and Di are higher in the SH polar region than NH polar regions.

The simulations are further compared with averaged observations at a similar horizontal scale of ~100 km. After applying 430-s running averages for observations, the average IWC and Ni values decrease by 0.5 – 1.5 orders of magnitude compared with 1-Hz observations depending on temperature and geographical region. Hemispheric differences are mostly consistent between 1-s and 430-s averaged observations except for polar regions. CAM6-nudg data show similar trend of average IWC, Ni and Di with respect to temperature as seen in observations, that is, the average IWC increases with increasing temperature consistent with previous observational studies (Krämer et al., 2016; Luebke et al., 2013; Schiller et al., 2008), average Ni shows no clear trend with temperature, and average Di increases with increasing temperature. Differing from observations, CAM6 produces the highest IWC and Ni in the tropical regions, followed by midlatitudes then polar regions for both hemispheres. The simulated IWC, Ni and Di also show~~s little~~ smaller differences between hemispheres and latitudes. The CAM6-nudg data underestimate and overestimate IWC in the NH and SH by 0.5 – 1 orders of magnitude, respectively, with the largest discrepancies in the midlatitudes. The simulations overestimate Ni in the tropics and polar regions in both hemispheres by 0.5 – 1 orders of magnitude, and overestimate Ni in the southern hemispheric midlatitude by 1 – 2 orders of magnitude. The simulated Di is about half of the observed values in most regions except polar regions. ~~Overall, the major problem of the simulation is the underestimation of average IWC by a factor of 2 – 10, which leads to the underestimation of average Di by a factor of 1.2 – 2. The comparison of Ni shows relatively better results, with the simulated average Ni being higher than observations in the tropics at -55ºC to -40ºC and in SH extratropical regions, but lower than observations in the NH midlatitude.~~ This result indicates "too many" and "too small" simulated ice in most regions~~, except for "too few" and "too small" simulated ice in the NH midlatitude~~. The ~~larger differences in average~~low bias of simulated Di ~~occur in the temperatures closer to -40ºC, which~~ indicates possible misrepresentation of ice particle growth and sedimentation ~~into the relatively warmer regions~~ in the model parameterization.

A sensitivity test is conducted by comparing 1-Hz observations with in-cloud quantities from model output (supplementary Figure S4). Larger differences are seen between simulated and observed IWC and Ni in Figure S4 compared with Figure 5. The directions (i.e., positive or negative) of model biases of IWC, Ni and Di are generally consistent in both comparisons.

A previous study by Righi et al. (2020) evaluated the ice microphysical properties in EMAC-MADE3 aerosol–climate model (i.e., ECHAM/MESSy Atmospheric Chemistry-Modal Aerosol Dynamics model for Europe adapted for global applications, 3rd generation) by comparing in-cloud quantities from model output with 1-Hz in situ observations of multiple aircraft field campaigns from 75ºN to 25ºS (Krämer et al., 2009, 2016, 2020). Although that study included more smaller ice particles (3 – 1280 μm) compared with this study, ~~That study~~they still showed low biases of simulated Di at 190 – 243 K, low biases of simulated IWC at 205 – 235 K, as well as high biases of simulated Ni above 225 K, which are generally in the same direction as the biases we found in CAM6 model. Note that Righi et al. (2020) implemented different cloud microphysics parameterizations compared with the CAM6 model, including a two-moment cloud microphysics scheme of Kuebbeler et al. (2014) and the ice nucleation parameterization for cirrus clouds (T < 238.15 K) from Kärcher et al. (2006) which account for both homogeneous and heterogeneous nucleation and the competition between the two mechanisms. More future intercomparison studies of these models are warranted to examine the reasons behind the similar biases.

3.2 RHi and σ_w distributions for in-cloud and clear-sky conditions

Regional distributions of RHi for clear-sky and in-cloud conditions are shown for 1-Hz observations (Figure 6), 430-s averaged observations (Figure 7) and simulations (Figure 8~~7~~). The 1-Hz o~~O~~bservations show RHi magnitudes ranging from < 5% up to ~180% in both clear-sky and in-cloud conditions, and mostly locate below the homogeneous freezing line except for the NH tropical region. A few samples exceed liquid saturation line but are within the measurement uncertainties of RHi. This result agrees with the RHi distributions based on previous midlatitudinal observations (Cziczo et al., 2013). Differing from 1-Hz observations, 430-s averaged observations show much lower RHi magnitudes for both clear-sky and in-cloud conditions, ranging from < 5% to 120% – 140%. For clear-sky conditions, the majority of the observed and simulated RHi values are below 100%, while the CAM6-nudg data show fewer RHi exceeding ice saturation. For in-cloud conditions, both 1-Hz observations and simulations show that RHi frequently occur within ~20% of ice saturation, consistent with previous observation and modeling studies (Diao et al., 2014a, 2017; D'Alessandro et al., 2017, 2019; Krämer et al., 2009), while almost no simulated RHi data exceed the homogeneous freezing threshold. The higher RHi observed in the NH tropical region was also observed by Krämer et al. (2009). Such feature can be explained by the competition between higher updrafts seen in the tropics and the depletion of water vapor from newly nucleated ice particles as discussed in Kärcher and Lohmann (2002). For the polar regions, in-cloud RHi is skewed towards ISS in both observations and simulations, indicating less effective water vapor depletion likely due to lower Ni values (Figure 5 e~~f~~). Note that the simulation samples in the tropical regions show peak frequencies at certain temperatures due to larger bin sizes of pressure levels in the lower latitudes.

Regional distributions of the variance of w (σ_w) for ~~in situ~~1-Hz observations at 40-s and 430-s scales and CAM6 nudged simulations are shown in Figures 9, 10~~8~~ and 11~~9~~, respectively. σ_w in the observations is calculated as the variance of w

within each ~~200~~ 40 and 430 seconds of data, which correspond~~s~~ to a horizontal scale of ~~4~~10 and 100~~6~~ km, respectively. ~~similar to the horizontal grid scale of the CAM6 simulations.~~ The σ_w in simulations is based on the "wsub" variable, which is calculated from the square root of turbulent kinetic energy (TKE) (Gettelman et al., 2010). Observed σ_w shows the highest values in the tropical and midlatitude regions reaching up to ~3 m/s, while the polar regions show updrafts up to ~1 m/s. A similar decreasing trend of maximum σ_w is seen in the simulations from the lower to higher latitudes. The observations show similar σ_w maximum values between clear-sky and in-cloud conditions, while the simulations show much higher maximum σ_w for in-cloud conditions in the tropics (1 m/s), midlatitude (1 m/s) and polar regions (0.5 m/s), compared with those values in clear sky (i.e., 0.~~2~~5, 0.25 and 0.1 m/s, respectively). This result suggests that the model has a~~s~~ stronger dependence on higher σ_w for cirrus cloud formation compared with observations. We further examine the potential impact of convection in simulations and observations. Supplementary Figure S5 shows the locations where w > 1 m/s is seen in the observations as well as where wsub > 0.5 m/s is seen in the CAM6-nudg data for in-cloud conditions. Since wsub in CAM6 is based on the turbulent scheme, higher wsub values indicate that the convection scheme may be active and produce detrained ice in convective outflows. The majority of observed and simulated in-cloud samples do not appear to have high w or wsub, indicating that detrained ice from the convection is unlikely a significant contribution. More future investigation is needed to track cirrus cloud origins and quantify impacts from convection.

4 Individual impacts of key controlling factors on cirrus clouds

4.1 Probability density functions of temperature, RHi and σ_w

PDFs of temperature, RHi and σ_w are shown in Figure 1~~2~~0. The PDFs are normalized by the total number of samples of both clear-sky and in-cloud conditions. The observations are located mostly around -68ºC to -40ºC, and the simulations show similar temperature distributions. For the PDFs of RHi, the observations and simulations all show peak position around~~t~~ 100% for in-cloud condition. However, a secondary peak is shown in simulations at 80% RHi, which is likely due to the parameter of RHi_{min} for ice cloud fraction calculation being set at 80% for representing variance of humidity in a grid box (more details on RHi_{min} are described in Gettelman et al. (2010)). In addition, the maximum RHi for in-cloud conditions are 170%, 154%, 160% and 257% for 1-Hz observations, 430-s averaged observations, CAM6-nudg and CAM6-free, respectively. The maximum RHi for clear-sky conditions are 175%, 135%, 108%, and 181%, respectively. ~~In addition, the maximum RHi values are 170% and 180% for in-cloud and clear-sky conditions in the observations, while the CAM-nudg simulations show lower values at 160% and 150%, respectively.~~ The CAM6-free data show higher maximum RHi values than CAM6-nudg data, likely due to additional data from tropical regions at temperatures below -70ºC (Figure 1~~2~~0 j~~e~~). When using a lower size cut-off (1 μm) of ice particles for the simulation data, the number of in-cloud samples increases by 4% (supplementary Figure S6~~1~~). However, negligible differences are seen in the PDFs of temperature, RHi and σ_w for the two simulations between Figures 1~~2~~0 and S6~~1~~. ~~Specifically, the steeper decrease of probability for RHi > 100% is consistently shown in the simulations regardless of the ice particle size range.~~

PDFs of σ_w show consistent results to Figures 9 – 11~~8 and 9~~, with simulations showing much higher maximum σ_w for in-cloud conditions than clear-sky conditions, ~~compared with the~~ while observations show similar maximum σ_w in both conditions. The lower maximum values of σ_w in simulations are most likely a result of model missing representations of gravity waves from topography, fronts, and convection, and only including σ_w from turbulence.

4.2 Effects of RHi and σ_w on ice microphysics

The relationships between ice microphysical properties and RHi are examined in Figure 13~~1~~. For the 1-Hz observations, the maximum IWC and Ni occur slightly above ice saturation at 110% RHi, while the maximum Di occur at 130% RHi. The average IWC and Ni increase 1.5 orders of magnitude from 40% to 110% RHi, and decrease~~s~~ 0.5 order of magnitude (i.e., a factor of 3) from 110% to 130% RHi. The maximum IWC and Ni do not occur at the highest RHi most likely due to the consumption of water vapor by ice deposition. High Di values at lower RHi (~30%) are likely a result of sedimenting large ice crystals, which has been previously observed by Diao et al. (2013) when investigating the evolutionary phases of cirrus clouds. For 430-s averaged observations, the peak IWC, Ni and Di occur at 100%, 100% and 115% RHi. The maximum IWC and Ni values are nearly the same between 1-s and 430-s averaged observations (i.e., 0.04 g/m^3 and 10 #/L, respectively) near saturation, while the 430-s averaged observations show lower minimum IWC and Ni at very low RHi (< 10%), which are 1.5 orders of magnitude lower than 1-Hz observations. This feature is due to in-cloud segments being longer around saturation compared with subsaturated conditions as shown in Diao et al. (2013), which means that less clear-sky conditions are being included in the 430-s averages around saturation and therefore show little reduction of the IWC and Ni due to spatial averaging.

In contrast to observations, both CAM6-nudg and CAM6-free simulations show bimodal distributions of IWC and Ni with the~~a~~ primary peak ~~of average IWC and Ni~~ at 108~~0~~% RHi and the~~a~~ secondary peak at 8~~10~~0% RHi~~, with a local minimum at 90% RHi~~. The secondary peak at RHi 80% is likely produced by the RHi_{min} parameter reflecting sub-grid scale RHi variance as mentioned above (Gettelman et al., 2010), which was set at the default value (80% RHi) for both simulations. The primary peak at 100% RHi is likely a result of the minimum threshold for heterogeneous ice nucleation being set at 120% as well as a sub-grid variability scaling factor 1.2 being considered (Wang et al., 2014a). ~~Similar to 430-s averaged observations, IWC and Ni show steep increase (i.e., 3 – 4 order of magnitude) from 60% to 100%. Smaller increases in IWC and Ni are shown in the simulations (i.e., 0.5 order of magnitude) compared with observations as RHi increases from 40% to 100%.~~ Similar to 430-s averaged observations, IWC and Ni show steep increase (i.e., 3 – 4 orders of magnitude) from 40% to 100%. Increases of average IWC and Ni are seen in the simulations as RHi increases from 12~~1~~0% to 16~~4~~0%, differing from the decreasing trend seen in the observations. These higher values of IWC and Ni near 160% are possibly due to RHi reaching the homogeneous nucleation thresholds, where ice nucleation becomes more dependent upon temperature and updraft speed (Liu and Penner, 2005). Note that at this same point as IWC and Ni increase, there is a decrease in Di, which also suggests homogeneous nucleation in the model. ~~The simulations may underestimate water vapor depletion rate since the average IWC and Ni in the simulations are lower than the observations by 0.5 order of magnitude at 110% – 140% RHi.~~ For Di - RHi

correlations, both simulations show similar results to the observations, with the maximum Di around 130% RHi and some large ice particles in the subsaturated conditions. The large variability of observed ice microphysical properties is also significantly underestimated in the model for ISS conditions. Standard deviations are 0.5 – 1 order of magnitude lower for IWC and Ni and a factor of 2 lower for Di compared with observations.

Comparing the correlations with σ_w (Figure 14~~2~~), the simulations show increasing IWC and Ni with higher σ_w, which agree with observations, ~~,~~ although the increase of IWC and Ni are smaller in the simulations than the 430-s observations. The simulated Di is relatively constant with increasing σ_w, which differs from the slight~~observed~~ positive correlation between Di and σ_w in the observations. This slight positive Di - σ_w correlation is likely due to the growth of ice particles as cirrus clouds evolve with continuous updrafts that supply excess water vapor above ice saturation, which was previously discussed in a cirrus cloud evolution analysis (Diao et al., 2013). The simulations may overlook this positive correlation due to several reasons, such as the lack of temporal resolution to resolve cirrus evolution in the growth phase, the lack of vertical velocity sub-grid variabilities (as discussed in Zhou et al. (2016)), and a dry bias (i.e., lower RHi) in the model (as discussed in Wu et al. (2017)).

Comparing the performance of two types of simulations, both CAM6-nudg and CAM6-free show bimodal distributions for IWC – RHi and Ni – RHi correlations, and they both show positive correlations for IWC – σ_w and Ni – σ_w. This result indicates that the general trends in these correlations are statistically robust and less affected by sampling sizes and geographical locations. For correlations with RHi, the maximum IWC value in CAM6-nudg and CAM6-free is lower than the 430-s averaged observations by a factor of 25 and 100, respectively. The maximum Ni value in CAM6-nudg is similar to the 430-s averaged observations, while that value in CAM6-free is lower by a factor of 3. For correlations with σ_w, there are no significant differences for the maximum IWC between the two simulation types. The maximum Ni value in CAM6-nudg and CAM6-free is higher than the 430-s averaged observations by a factor of 3 and 10, respectively. These results show that CAM6-nudg data, which are collocated with flight tracks, produce IWC and Ni values closer to the 430-s averaged observations than CAM6-free, possibly due to the variabilities of IWC and Ni in different geographical locations as shown in Figure 5.

4.3 Aerosol indirect effects

The effects of larger and smaller aerosols (i.e., Na_{500} and Na_{100}) on ice microphysical properties are further examined for observations and CAM6-nudg data (Figures 15 and 16~~3~~). Cloud fraction is calculated in each temperature – Na bin by normalizing the number of in-cloud samples with the total number of samples in that bin for both observations and simulations. For three cirrus microphysical properties (i.e., IWC, Ni and Di), positive correlations are seen in 1-Hz observations with respect to Na_{500} and Na_{100}. In addition, higher Na_{500} (>10 cm^{-3}) and Na_{100} (>100 cm^{-3}) values are associated with significant increases in cloud fraction. At -70ºC to -60ºC, higher IWC, Ni and cloud fraction are seen when Na_{500} is observed, with positive correlations of IWC and Ni with respect to Na_{500}. This finding indicates that larger aerosols provide an effective pathway of ice particle formation for colder conditions. The higher IWC and Ni are only shown in much

higher Na_{100} (>100 cm^{-3}) between -70ºC and -60ºC, demonstrating that larger aerosols facilitate ice formation more effectively than smaller aerosols at this temperature range, possibly due to the activation of larger aerosols as INPs for heterogeneous nucleation. Compared with 1-Hz observations, 430-s averaged observations show weaker correlations of IWC, Ni and Di with respect to Na. However, they do still show higher IWC and Ni between -70ºC and -40ºC associated with higher Na (i.e., Na_{500} > 1 cm^{-3} and Na_{100} > 30 cm^{-3}).

The CAM6-nudg simulation shows increasing average IWC, average Ni and cloud fraction with increasing Na_{500}, consistent with the observations. But at temperatures below -60ºC, simulated IWC and Ni do not show a sudden increase ~~when~~ with higher Na_{500} ~~exists~~ as shown in the observations. The simulated Di slightly decreases with increasing Na_{500}, differing from the increasing trend seen in observations. For aerosol indirect effect analysis based on Na_{100}, the comparison results are similar to Na_{500}, that is, CAM6-nudg simulation is able to represent positive correlations of IWC, Ni and cloud fraction with respect to Na_{100}.~~,~~ However, CAM6-nudg simulation shows smaller (larger) increase of IWC (Ni) at very high Na (i.e., Na_{500} > 1.6 cm^{-3} and Na_{100} > 30 cm^{-3}) compared with the 430-s averaged observations. The model also ~~but underestimates the average IWC, underestimates Ni below -60ºC, and~~ misses positive correlations between Di and Na_{100}~~.~~ seen in both 1-Hz and 430-s averaged observations.

5 Discussion and conclusions

In this study, we investigate the statistical distributions of cirrus cloud microphysical properties (i.e., IWC, Ni, and Di) as well as several key controlling factors (i.e., temperature, RHi, σ_w and Na) using a comprehensive in situ observational dataset and GCM simulations. Regional variations of cirrus cloud microphysical properties are examined for six latitudinal regions in two hemispheres. Two types of CAM6 simulations are evaluated, i.e., nudged and free-running simulations.

Regarding the regional variations in 1-Hz observations~~at warmer conditions (i.e., -55ºC to -40ºC)~~, the highest and lowest IWC values were observed in NH midlatitude and SH midlatitude, respectively, while the polar regions show the lowest Ni and highest Di at warmer conditions (i.e., -55ºC to -40ºC) (Figure~~s 4 and~~ 5). The hemispheric differences between NH and SH midlatitudes indicate a possible role of anthropogenic aerosols and/or land-sea contrast in controlling ice microphysical properties. Thermodynamic and dynamic conditions can also affect nucleation mechanisms. For example, t~~T~~he tropical regions show the highest IWC and Ni at temperatures below -55ºC possibly due to convection anvils with the droplet freezing from down below or homogeneous nucleation in gravity waves generated by convection. This feature is corroborated by the fact that tropical regions show the highest RHi values for both clear-sky and in-cloud conditions (Figure 6), while the midlatitude and polar regions show fewer samples exceeding the homogeneous nucleation threshold. The higher RHi values in tropics are likely contributed by higher updrafts (indicated by higher σ_w in Figure 9~~8~~). These results demonstrate the important roles of these controlling factors on cirrus clouds at different latitudinal and temperature ranges.

Evaluating the model simulations of cirrus microphysical properties, different model performance results are seen in different regions. For example, simulations underestimated the IWC ~~and Ni~~ in NH ~~midlatitude~~ (Figure~~s 4 and~~ 5), possibly

due to model dry bias to form ice clouds (as discussed in Wu et al. (2017)) and/or smaller aerosol indirect effects on IWC ~~and Ni~~ in the simulations (Figures 15 and 16~~3~~). For RHi distributions, ~~the~~ both simulations represent a similar peak position at ice saturation for in-cloud RHi PDFs compared with observations but CAM6-nudg underestimates the frequency and magnitude of ISS for clear-sky condition. For σ_w distributions, simulations represent similar regional variations of σ_w compared with observations, with σ_w decreasing from lower to higher latitudes. ~~However, larger biases are seen in the simulations for~~ The model performs well for representing the effects of RHi and σ_w on ice microphysical properties, specifically for showing the maximum IWC and Ni at 100% RHi, and the positive correlations with σ_w. ~~including~~ Some differences include the simulated average IWC and Ni ~~maximize~~ showing a secondary peak position at 80% RHi, likely due to the minimum RHi threshold used in the model parameterization ~~instead of 110% RHi as observed, and the simulation misses the increasing average Di with increasing σ_w as observed~~. Both simulation types show similar correlation trends of ice microphysical properties with respect to RHi and σ_w. CAM6-nudg performs better for representing IWC and Ni magnitudes than CAM6-free, possibly due to better collocation between CAM6-nudg and observations.

For aerosol indirect effects, the simulations underestimate IWC, Ni, Di as well as cloud fraction at colder conditions (< -60ºC) when larger aerosols exist, indicating that the effectiveness of larger aerosols is underestimated at the colder conditions. The observations also show higher Di than simulations by a factor of 3 – 4 at warmer temperatures (-50ºC to -40ºC), indicating misrepresentation of ~~inefficient~~ ice particle growth and/or sedimentation in the simulations. In addition, the ~~observed~~ IWC, Ni and Di in 430-s averaged observations show ~~significant~~ increase at higher Na_{500} (>1~~0~~ cm^{-3}) and Na_{100} (>3~~10~~0 cm^{-3}), while simulations ~~do not show such~~only show significant increase of Ni. This result indicates that aerosol indirect effects may be underestimated especially for higher Na values. It is possible that small ice crystals < 62.5 μm may have formed under high Na but are excluded due to the size constraint. Additionally, because INP activation is highly dependent upon temperature, we acknowledge the limitation of using Na_{500} to indicate INP concentrations. The assumption of ice mass and dimension relationship from Brown and Francis (1995) may also lead to uncertainties due to various ice habits. These caveats call for more investigation on small ice measurements, INP measurements at temperature ≤ -40°C, and measurements of various ice habits.

Overall, the global-scale observational dataset used in this study provides statistically robust distributions of cirrus cloud microphysical properties, which can be used to evaluate the effects of thermodynamics, dynamics and aerosols on cirrus clouds in a global climate model. Extending from previous studies that investigated climate model sensitivity to individual cirrus cloud controlling factors, i.e., w (Shi and Liu, 2016), RHi (D'Alessandro et al., 2019), water vapor (Wu et al., 2017), and aerosols (Wang et al., 2014a), this study provides an ~~comprehensive~~ analysis of all factors. In addition, further attention was given towards evaluating these factors in the simulations based on geographical locations. For both observations and simulations, higher ice supersaturations and stronger vertical motions are shown in tropical and midlatitude regions, which possibly lead to increased homogeneous nucleation and convection-generated cirrus, consistent with higher IWC and Ni and lower Di in these regions compared with polar regions. In addition, underestimating aerosol indirect effects in the simulations likely contributes to the underestimation of IWC in the NH. Even though small ice particles (< 62.5 μm) are

excluded in this study, correlations between ice microphysical properties and these key controlling factors are still clearly seen in the observation dataset. In addition, using two methods that compare observations on the horizontal scales of 230 m and 100 km with simulations, both methods show similar signs for model biases of IWC, Ni and Di, while smaller model biases are seen when comparing against the coarser resolution observations. This study underscores the importance of correctly representing the thermodynamic, dynamic and aerosol conditions in climate models at various regions, as well as accurately simulating their correlations with ice microphysical properties. Failing to do so may result in biases of cirrus cloud microphysical properties depending on different regions and temperatures, leading to biases in cirrus cloud radiative effects on a global scale.

Data Availability

Observations from the seven NSF flight campaigns are accessible at https://data.eol.ucar.edu/.

Author contributions

R. Patnaude and M. Diao contributed to the development of the ideas, conducted quality control to aircraft-based observations, and wrote the majority of the manuscript. R. Patnaude contributed to all model simulations and the subsequent data analysis. X. Liu and S. Chu provided expertise on the set-up of CAM6 model simulations and provided input to the analysis of simulation data.

Competing interests

The authors declare that they have no conflict of interest.

Acknowledgments

R. Patnaude and M. Diao acknowledge funding support from U. S. National Science Foundation grants AGS-1642291 and OPP-1744965. R. Patnaude also acknowledges support from the San Jose State University Walker Fellowship. For funding support in 2016 and 2018 summer, M. Diao acknowledges the NCAR Advanced Study Program (ASP) Faculty Fellowship. X. Liu and S. Chu acknowledge the support of the National Science Foundation under grant AGS-1642289 / 2001903. We would like to acknowledge the NCAR/Earth Observation Laboratory flight teams from the seven flight campaigns: START08, HIPPO, PREDICT, DC3, CONTRAST, TORERO, and ORCAS. For in situ observations of water vapor by the VCSEL hygrometer, field support, calibration and QA/QC was conducted by M. Diao, J. DiGangi, M. Zondlo, and S. Beaton. Additional appreciation is given to Jorgen Jensen, Chris Webster, and Christina McCluskey for helpful discussions.

References

Barth, M. C., Cantrell, C. A., Brune, W. H., Rutledge, S. A., Crawford, J. H., Huntrieser, H., Carey, L. D., MacGorman, D., Weisman, M., Pickering, K. E., Bruning, E., Anderson, B., Apel, E., Biggerstaff, M., Campos, T., Campuzano-Jost, P., Cohen, R., Crounse, J., Day, D. A., Diskin, G., Flocke, F., Fried, A., Garland, C., Heikes, B., Honomichl, S., Hornbrook, R., Gregory Huey, L., Jimenez, J. L., Lang, T., Lichtenstern, M., Mikoviny, T., Nault, B., O'Sullivan, D., Pan, L. L., Peischl, J., Pollack, I., Richter, D., Riemer, D., Ryerson, T., Schlager, H., St. Clair, J., Walega, J., Weibring, P., Weinheimer, A., Wennberg, P., Wisthaler, A., Wooldridge, P. J. and Ziegler, C.: The Deep Convective Clouds and Chemistry (DC3) field campaign, Bull. Am. Meteorol. Soc., 96(8), 1281–1310, doi:10.1175/BAMS-D-13-00290.1, 2015.

Bogenschutz, P. A., Gettelman, A., Morrison, H., Larson, V. E., Craig, C. and Schanen, D. P.: Higher-order turbulence closure and its impact on climate simulations in the community atmosphere model, J. Clim., 26(23), 9655–9676, doi:10.1175/JCLI-D-13-00075.1, 2013.

Boucher, O., Randall, D., Artaxo, P., Bretherton, C., Feingold, G., Forster, P., Kerminen, V.-M., Kondo, Y., Liao, H., Lohmann, U., Rasch, P., Satheesh, S. K., Sherwood, S. C., Stevens, B. and Zhang, X.-Y.: Clouds and aerosols, Clim. Chang. 2013 Phys. Sci. Basis Work. Gr. I Contrib. to Fifth Assess. Rep. Intergov. Panel Clim. Chang., 9781107057(July), 571–658, doi:10.1017/CBO9781107415324.016, 2013.

Brown, P. R. A. and Francis, P. N.: Improved Measurements of the Ice Water Content in Cirrus Using a Total-Water Probe, J. Atmos. Ocean. Technol., 12, 410–414, doi:10.1175/1520-0426(1995)012%3C0410:IMOTIW%3E2.0.CO;2, 1995.

Chylek, P., Dubey, M. K., Lohmann, U., Ramanathan, V., Kaufman, Y. J., Lesins, G., Hudson, J., Altmann, G. and Olsen, S.: Aerosol indirect effect over the Indian Ocean, Geophys. Res. Lett., 33(6), L06806, doi:10.1029/2005GL025397, 2006.

Cziczo, D. J. and Froyd, K. D.: Sampling the composition of cirrus ice residuals, Atmos. Res., 142, 15–31, doi:10.1016/j.atmosres.2013.06.012, 2014.

Cziczo, D. J., Froyd, K. D., Hoose, C., Jensen, E. J., Diao, M., Zondlo, M. A., Smith, J. B., Twohy, C. H. and Murphy, D. M.: Clarifying the dominant sources and mechanisms of cirrus cloud formation, Science (80-.)., 340(6138), 1320–1324, doi:10.1126/science.1234145, 2013.

D'Alessandro, J. J., Diao, M., Wu, C., Liu, X., Chen, M., Morrison, H., Eidhammer, T., Jensen, J. B., Bansemer, A., Zondlo, M. A. and DiGangi, J. P.: Dynamical conditions of ice supersaturation and ice nucleation in convective systems: A comparative analysis between in situ aircraft observations and WRF simulations, J. Geophys. Res., 122(5), 2844–2866, doi:10.1002/2016JD025994, 2017.

D'Alessandro, J. J., Diao, M., Wu, C., Liu, X., Jensen, J. B. and Stephens, B. B.: Cloud phase and relative humidity distributions over the Southern Ocean in austral summer based on in situ observations and CAM5 simulations, J. Clim., 32(10), 2781–2805, doi:10.1175/JCLI-D-18-0232.1, 2019.

DeMott, P. J., Prenni, A. J., Liu, X., Kreidenweis, S. M., Petters, M. D., Twohy, C. H., Richardson, M. S., Eidhammer, T. and Rogers, D. C.: Predicting global atmospheric ice nuclei distributions and their impacts on climate, Proc. Natl. Acad. Sci., 107(25), 11217–11222, doi:10.1073/pnas.0910818107, 2010.

Diao, M., Zondlo, M. A., Heymsfield, A. J., Beaton, S. P. and Rogers, D. C.: Evolution of ice crystal regions on the microscale based on in situ observations, Geophys. Res. Lett., 40(13), 3473–3478, doi:10.1002/grl.50665, 2013.

Diao, M., Zondlo, M. A., Heymsfield, A. J., Avallone, L. M., Paige, M. E., Beaton, S. P., Campos, T. and Rogers, D. C.: Cloud-scale ice-supersaturated regions spatially correlate with high water vapor heterogeneities, Atmos. Chem. Phys., 14(5), 2639–2656, doi:10.5194/acp-14-2639-2014, 2014a.

Diao, M., Zondlo, M. A., Heymsfield, A. J. and Beaton, S. P.: Hemispheric comparison of cirrus cloud evolution using in situ measurements in HIAPER Pole-to-Pole Observations, Geophys. Res. Lett., 41(11), 1–8, doi:10.1002/2014GL059873, 2014b.

Diao, M., Jensen, J. B., Pan, L. L., Homeyer, C. R., Honomichl, S., Bresch, J. F. and Bansemer, A.: Distributions of ice supersaturation and ice crystals from airborne observations in relation to upper tropospheric dynamical boundaries, J. Geophys. Res., 120(10), 5101–5121, doi:10.1002/2015JD023139, 2015.

Diao, M., Bryan, G. H., Morrison, H. and Jensen, J. B.: Ice nucleation parameterization and relative humidity distribution in idealized squall-line simulations, J. Atmos. Sci., 74(9), 2761–2787, doi:10.1175/JAS-D-16-0356.1, 2017.

Eidhammer, T., Morrison, H., Bansemer, A., Gettelman, A. and Heymsfield, A. J.: Comparison of ice cloud properties simulated by the Community Atmosphere Model (CAM5) with in-situ observations, Atmos. Chem. Phys., 14(18), 10103–10118, doi:10.5194/acp-14-10103-2014, 2014.

Eidhammer, T., Morrison, H., Mitchell, D., Gettelman, A. and Erfani, E.: Improvements in global climate model microphysics using a consistent representation of ice particle properties, J. Clim., 30(2), 609–629, doi:10.1175/JCLI-D-16-0050.1, 2017.

Gelaro, R., McCarty, W., Suárez, M. J., Todling, R., Molod, A., Takacs, L., Randles, C. A., Darmenov, A., Bosilovich, M. G., Reichle, R., Wargan, K., Coy, L., Cullather, R., Draper, C., Akella, S., Buchard, V., Conaty, A., da Silva, A. M., Gu, W., Kim, G. K., Koster, R., Lucchesi, R., Merkova, D., Nielsen, J. E., Partyka, G., Pawson, S., Putman, W., Rienecker, M., Schubert, S. D., Sienkiewicz, M. and Zhao, B.: The modern-era retrospective analysis for research and applications, version 2 (MERRA-2), J. Clim., 30(14), 5419–5454, doi:10.1175/JCLI-D-16-0758.1, 2017.

Gettelman, A. and Morrison, H.: Advanced two-moment bulk microphysics for global models. Part I: Off-line tests and comparison with other schemes, J. Clim., 28(3), 1268–1287, doi:10.1175/JCLI-D-14-00102.1, 2015.

Gettelman, A., Liu, X., Ghan, S. J., Morrison, H., Park, S., Conley, A. J., Klein, S. A., Boyle, J., Mitchell, D. L. and Li, J. L. F.: Global simulations of ice nucleation and ice supersaturation with an improved cloud scheme in the Community Atmosphere Model, J. Geophys. Res. Atmos., 115(18), 1–19, doi:10.1029/2009JD013797, 2010.

Gettelman, A., Bardeen, C. G., McCluskey, C. S., Järvinen, E., Stith, J., Bretherton, C., et al. (2020). Simulating Observations of Southern Ocean Clouds and Implications for Climate. *Journal of Geophysical Research: Atmospheres*,

125, e2020JD032619. https://doi.org/10.1029/2020JD032619

Golaz, J. C., Larson, V. E. and Cotton, W. R.: A PDF-Based Model for Boundary Layer Clouds. Part I : Method and Model Description, J. Atmos. Sci., 59, 3540–3551, 2002.

Heymsfield, A. J.: Precipitation Development in Stratiform Ice Clouds: A Microphysical and Dynamical Study, J. Atmos. Sci., 367–381, 1977.

Heymsfield, A. J., Winker, D. and van Zadelhoff, G. J.: Extinction-ice water content-effective radius algorithms for CALIPSO, Geophys. Res. Lett., 32(10), 1–4, doi:10.1029/2005GL022742, 2005.

Heymsfield, A. J., Krämer, M., Wood, N. B., Gettelman, A., Field, P. R. and Liu, G.: Dependence of the Ice Water Content and Snowfall Rate on Temperature, Globally: Comparison of in Situ Observations, Satellite Active Remote Sensing Retrievals, and Global Climate Model Simulations, J. Appl. Meteorol. Climatol., 56(190), 189–215, doi:10.1175/JAMC-D-16-0230.1, 2017.

Hoose, C., Kristjánsson, J. E., Chen, J. P. and Hazra, A.: A classical-theory-based parameterization of heterogeneous ice nucleation by mineral dust, soot, and biological particles in a global climate model, J. Atmos. Sci., 67(8), 2483–2503, doi:10.1175/2010JAS3425.1, 2010.

Jensen, E. J., Toon, O. B., Vay, S. A., Ovarlez, J., May, R., Bui, T. P., Twohy, C. H., Gandrud, B. W., Pueschel, R. F. and Schumann, U.: Prevalence of ice-supersaturated regions in the upper troposphere: Implications for optically thin ice cloud formation, J. Geophys. Res. Atmos., 106(D15), 17253–17266, doi:10.1029/2000JD900526, 2001.

Kanitz, T., Seifert, P., Ansmann, A., Engelmann, R., Althausen, D., Casiccia, C. and Rohwer, E. G.: Contrasting the impact of aerosols at northern and southern midlatitudes on heterogeneous ice formation, Geophys. Res. Lett., 38(17), 1–5, doi:10.1029/2011GL048532, 2011.

Kärcher, B. and Lohmann, U.: A parameterization of cirrus cloud formation: Homogeneous freezing of supercooled aerosols, J. Geophys. Res., 107(D2), doi:10.1029/2001JD000470, 2002.

Kärcher, B. and Lohmann, U.: A parameterization of cirrus cloud formation: Heterogeneous freezing, J. Geophys. Res., 107(D14), 4402, doi:10.1029/2002JD003220, 2003.

Kärcher, B., Hendricks, J. and Lohmann, U.: Physically based parameterization of cirrus cloud formation for use in global atmospheric models, J. Geophys. Res. Atmos., 111, D01205, doi:10.1029/2005JD006219, 2006.

Koop, T., Luo, B., Tsias, A. and Peter, T.: Water activity as the determinant for homogeneous ice nucleation in aqueous solutions, Nature, 406(6796), 611–614, doi:10.1038/35020537, 2000.

Kooperman, G. J., Pritchard, M. S., Ghan, S. J., Wang, M., Somerville, R. C. J. and Russell, L. M.: Constraining the influence of natural variability to improve estimates of global aerosol indirect effects in a nudged version of the Community Atmosphere Model 5, J. Geophys. Res. Atmos., 117(23), 1–16, doi:10.1029/2012JD018588, 2012.

Krämer, M., Schiller, C., Afchine, A., Bauer, R., Gensch, I., Mangold, A., Schlicht, S., Spelten, N., Sitnikov, N., Borrmann, S., De Reus, M. and Spichtinger, P.: Ice supersaturations and cirrus cloud crystal numbers, Atmos. Chem. Phys., 9(11), 3505–3522, doi:10.5194/acp-9-3505-2009, 2009.

Krämer, M., Rolf, C., Luebke, A., Afchine, A., Spelten, N., Costa, A., Meyer, J., Zöger, M., Smith, J., Herman, R. L., Buchholz, B., Ebert, V., Baumgardner, D., Borrmann, S., Klingebiel, M. and Avallone, L.: A microphysics guide to cirrus clouds − Part 1: Cirrus types, Atmos. Chem. Phys., 16(5), 3463–3483, doi:10.5194/acp-16-3463-2016, 2016.

Krämer, M., Rolf, C., Spelten, N., Afchine, A., Fahey, D., Jensen, E., Khaykin, S., Kuhn, T., Lawson, P., Lykov, A., Pan, L. L., Riese, M., Rollins, A., Stroh, F., Thornberry, T., Wolf, V., Woods, S., Spichtinger, P., Quaas, J. and Sourdeval, O.: A Microphysics Guide to Cirrus – Part II : Climatologies of Clouds and Humidity from Observations, Atmos. Chem. Phys. Discuss., (January), 2020.

Kuebbeler, M., Lohmann, U., Hendricks, J. and Kärcher, B.: Dust ice nuclei effects on cirrus clouds, Atmos. Chem. Phys., 14(6), 3027–3046, doi:10.5194/acp-14-3027-2014, 2014.

Lin, S. J.: A "vertically Lagrangian" finite-volume dynamical core for global models, Mon. Weather Rev., 132(10), 2293–2307, doi:10.1175/1520-0493(2004)132<2293:AVLFDC>2.0.CO;2, 2004.

Liu, X. and Penner, J. E.: Ice nucleation parameterization for global models, Meteorol. Zeitschrift, 14(4), 499–514, doi:10.1127/0941-2948/2005/0059, 2005.

Liu, X., Penner, J. E., Ghan, S. J. and Wang, M.: Inclusion of ice microphysics in the NCAR Community Atmospheric Model version 3 (CAM3), J. Clim., 20(18), 4526–4547, doi:10.1175/JCLI4264.1, 2007.

Liu, X., Shi, X., Zhang, K., Jensen, E. J., Gettelman, A., Barahona, D., Nenes, A. and Lawson, P.: Sensitivity studies of dust ice nuclei effect on cirrus clouds with the community atmosphere model CAM5, Atmos. Chem. Phys., 12(24), 12061–12079, doi:10.5194/acp-12-12061-2012, 2012.

Liu, X., Ma, P. L., Wang, H., Tilmes, S., Singh, B., Easter, R. C., Ghan, S. J. and Rasch, P. J.: Description and evaluation of a new four-mode version of the Modal Aerosol Module (MAM4) within version 5.3 of the Community Atmosphere Model, Geosci. Model Dev., 9(2), 505–522, doi:10.5194/gmd-9-505-2016, 2016.

Luebke, A. E., Avallone, L. M., Schiller, C., Meyer, J., Rolf, C. and Krämer, M.: Ice water content of Arctic, midlatitude, and tropical cirrus - Part 2: Extension of the database and new statistical analysis, Atmos. Chem. Phys., 13(13), 6447–6459, doi:10.5194/acp-13-6447-2013, 2013.

Luebke, A. E., Afchine, A., Costa, A., Grooß, J. U., Meyer, J., Rolf, C., Spelten, N., M Avallone, L., Baumgardner, D. and Krämer, M.: The origin of midlatitude ice clouds and the resulting influence on their microphysical properties, Atmos. Chem. Phys., 16(9), 5793–5809, doi:10.5194/acp-16-5793-2016, 2016.

Mace, G. G. and Wrenn, F. J.: Evaluation of the hydrometeor layers in the East and West Pacific within ISCCP cloud-top pressure-optical depth bins using merged CloudSat and CALIPSO data, J. Clim., 26(23), 9429–9444, doi:10.1175/JCLI-D-12-00207.1, 2013.

Mcfarquhar, G. M. and Heymsfield, A. J.: Parameterization of tropical cirrus ice crystal size distributions and implications for radiative transfer: Results from CEPEX, J. Atmos. Sci., 54(17), 2187–2200, doi:10.1175/1520-0469(1997)054<2187:POTCIC>2.0.CO;2, 1997.

Minikin, A., Petzold, A., Ström, J., Krejci, R., Seifert, M., van Velthoven, P., Schlager, H. and Schumann, U.: Aircraft

observations of the upper tropospheric fine particle aerosol in the Northern and Southern Hemispheres at midlatitudes, Geophys. Res. Lett., 30(10), doi:10.1029/2002gl016458, 2003.

Mitchell, D. L., Garnier, A., Pelon, J. and Erfani, E.: CALIPSO (IIR-CALIOP) retrievals of cirrus cloud ice-particle concentrations, Atmos. Chem. Phys., 18(23), 17325–17354, doi:10.5194/acp-18-17325-2018, 2018.

Montgomery, M. T., Davis, C., Dunkerton, T., Wang, Z., Velden, C., Torn, R., Majumdar, S. J., Zhang, F., Smith, R. K., Bosart, L., Bell, M. M., Haase, J. S., Heymsfield, A., Jensen, J., Campos, T. and Boothe, M. A.: The pre-depression investigation of cloud-systems in the tropics (PREDICT) experiment: Scientific basis, new analysis tools, and some first results, Bull. Am. Meteorol. Soc., 93(2), 153–172, doi:10.1175/BAMS-D-11-00046.1, 2012.

Morrison, H. and Gettelman, A.: A new two-moment bulk stratiform cloud microphysics scheme in the community atmosphere model, version 3 (CAM3). Part I: Description and numerical tests, J. Clim., 21(15), 3642–3659, doi:10.1175/2008JCLI2105.1, 2008.

Muhlbauer, A., Ackerman, T. P., Comstock, J. M., Diskin, G. S., Evans, S. M., Lawson, R. P. and Marchand, R. T.: Impact of large-scale dynamics on the microphysical properties of midlatitude cirrus, J. Geophys. Res., 119(7), 3976–3996, doi:10.1002/2013JD020035, 2014a.

Muhlbauer, A., Kalesse, H. and Kollias, P.: Vertical velocities and turbulence in midlatitude anvil cirrus: A comparison between in situ aircraft measurements and ground-based Doppler cloud radar retrievals, Geophys. Res. Lett., 41(22), 7814–7821, doi:10.1002/2014GL062279, 2014b.

Murphy, D. M. and Koop, T.: Review of the vapour pressures of ice and supercooled water for atmospheric applications, Q. J. R. Meteorol. Soc., 131(608), 1539–1565, doi:10.1256/qj.04.94, 2005.

Pan, L. L., Bowman, K. P., Atlas, E. L., Wofsy, S. C., Zhang, F., Bresch, J. F., Ridley, B. A., Pittman, J. V., Homeyer, C. R., Romashkin, P. and Cooper, W. A.: The stratosphere-troposphere analyses of regional transport 2008 experiment, Bull. Am. Meteorol. Soc., 91(3), 327–342, doi:10.1175/2009BAMS2865.1, 2010.

Pan, L. L., Atlas, E. L., Salawitch, R. J., Honomichl, S. B., Bresch, J. F., Randel, W. J., Apel, E. C., Hornbrook, R. S., Weinheimer, A. J., Anderson, D. C., Andrews, S. J., Baidar, S., Beaton, S. P., Campos, T. L., Carpenter, L. J., Chen, D., Dix, B., Donets, V., Hall, S. R., Hanisco, T. F., Homeyer, C. R., Huey, L. G., Jensen, J. B., Kaser, L., Kinnison, D. E., Koenig, T. K., Lamarque, J.-F., Liu, C., Luo, J., Luo, Z. J., Montzka, D. D., Nicely, J. M., Pierce, R. B., Riemer, D. D., Robinson, T., Romashkin, P., Saiz-Lopez, A., Schauffler, S., Shieh, O., Stell, M. H., Ullmann, K., Vaughan, G., Volkamer, R. and Wolfe, G.: The Convective Transport of Active Species in the Tropics (CONTRAST) Experiment, Bull. Am. Meteorol. Soc., 98(1), 106–128, doi:10.1175/bams-d-14-00272.1, 2017.

Patnaude, R. and Diao, M.: Aerosol indirect effects on cirrus clouds based on global aircraft observations, Geophys. Res. Lett., 47, doi:10.1029/2019gl086550, 2020.

Penner, J. E., Chen, Y., Wang, M. and Liu, X.: Possible influence of anthropogenic aerosols on cirrus clouds and anthropogenic forcing, Atmos. Chem. Phys., 9(3), 879–896, doi:10.5194/acp-9-879-2009, 2009.

Penner, J. E., Zhou, C., Garnier, A. and Mitchell, D. L.: Anthropogenic Aerosol Indirect Effects in Cirrus Clouds, J.

Geophys. Res. Atmos., 123(20), 11,652-11,677, doi:10.1029/2018JD029204, 2018.

Prenni, A. J., Petters, M. D., Faulhaber, A., Carriço, C. M., Ziemann, P. J., Kreidenweis, S. M. and DeMott, P. J.: Heterogeneous ice nucleation measurements of secondary organic aerosol generated from ozonolysis of alkenes, Geophys. Res. Lett., 36(6), 1–5, doi:10.1029/2008GL036957, 2009.

Righi, M., Hendricks, J., Lohmann, U., Gerhard Beer, C., Hahn, V., Heinold, B., Heller, R., Krämer, M., Ponater, M., Rolf, C., Tegen, I. and Voigt, C.: Coupling aerosols to (cirrus) clouds in the global EMAC-MADE3 aerosol-climate model, Geosci. Model Dev., 13(3), 1635–1661, doi:10.5194/gmd-13-1635-2020, 2020.

Sassen, K., Wang, Z. and Liu, D.: Global distribution of cirrus clouds from CloudSat/cloud-aerosol lidar and infrared pathfinder satellite observations (CALIPSO) measurements, J. Geophys. Res. Atmos., 113(8), 1–12, doi:10.1029/2008JD009972, 2008.

Schiller, C., Krämer, M., Afchine, A., Spelten, N. and Sitnikov, N.: Ice water content of Arctic, midlatitude, and tropical cirrus, J. Geophys. Res. Atmos., 113(D24), 1–12, doi:10.1029/2008JD010342, 2008.

Shi, X. and Liu, X.: Effect of cloud-scale vertical velocity on the contribution of homogeneous nucleation to cirrus formation and radiative forcing, Geophys. Res. Lett., 43(12), 6588–6595, doi:10.1002/2016GL069531, 2016.

Shi, X., Liu, X. and Zhang, K.: Effects of pre-existing ice crystals on cirrus clouds and comparison between different ice nucleation parameterizations with the Community Atmosphere Model (CAM5), Atmos. Chem. Phys., 15, 1503–1520, doi:10.5194/acp-15-1503-2015, 2015.

Stephens, B. B., Long, M. C., Keeling, R. F., Kort, E. A., Sweeney, C., Apel, E. C., Atlas, E. L., Beaton, S., Bent, J. D., Blake, N. J., Bresch, J. F., Casey, J., Daube, B. C., Diao, M., Diaz, E., Dierssen, H., Donets, V., Gao, B.-C., Gierach, M., Green, R., Haag, J., Hayman, M., Hills, A. J., Hoecker-Martínez, M. S., Honomichl, S. B., Hornbrook, R. S., Jensen, J. B., Li, R.-R., McCubbin, I., McKain, K., Morgan, E. J., Nolte, S., Powers, J. G., Rainwater, B., Randolph, K., Reeves, M., Schauffler, S. M., Smith, K., Smith, M., Stith, J., Stossmeister, G., Toohey, D. W. and Watt, A. S.: The O2/N2 Ratio and CO2 Airborne Southern Ocean Study, Bull. Am. Meteorol. Soc., 99(2), 381–402, doi:10.1175/BAMS-D-16-0206.1, 2018.

Stephens, G. and Webster, P.: Clouds and climate: Sensitivity of simple systems, J. Atmos. Sci., 38, 235–247, 1981.

Storelvmo, T. and Herger, N.: Cirrus cloud susceptibility to the injection of ice nuclei in the upper troposphere, J. Geophys. Res., 119(5), 2375–2389, doi:10.1002/2013JD020816, 2014.

Tan, X., Huang, Y., Diao, M., Bansemer, A., Zondlo, M. A., DiGangi, J. P., Volkamer, R. and Hu, Y.: An assessment of the radiative effects of ice supersaturation based on in situ observations, Geophys. Res. Lett., 43(20), 11,039-11,047, doi:10.1002/2016GL071144, 2016.

Thorsen, T. J., Fu, Q., Comstock, J. M., Sivaraman, C., Vaughan, M. A., Winker, D. M., and Turner, D. D.: Macrophysical properties of tropical cirrus clouds from the CALIPSO satellite and from ground-based micropulse and Raman lidars, J. Geophys. Res. Atmos., 118, 9209– 9220, doi:10.1002/jgrd.50691, 2013.

Tseng, H.-H. and Fu, Q.: Temperature control of the variability of tropical tropopause layer cirrus clouds. Journal of

Geophysical Research: Atmospheres, 122, 11,062–11,075. https://doi.org/10.1002/2017JD027093, 2017.

Volkamer, R., Baidar, S., Campos, T. L., Coburn, S., DiGangi, J. P., Dix, B., Eloranta, E. W., Koenig, T. K., Morley, B., Ortega, I., Pierce, B. R., Reeves, M., Sinreich, R., Wang, S., Zondlo, M. A. and Romashkin, P. A.: Aircraft measurements of BrO, IO, glyoxal, NO2, H2O, O2-O2 and aerosol extinction profiles in the tropics: Comparison with aircraft-/ship-based in situ and lidar measurements, Atmos. Meas. Tech., 8(5), 2121–2148, doi:10.5194/amt-8-2121-2015, 2015.

Wang, M. and Penner, J. E.: Cirrus clouds in a global climate model with a statistical cirrus cloud scheme, Atmos. Chem. Phys., 10(12), 5449–5474, doi:10.5194/acp-10-5449-2010, 2010.

Wang, M., Liu, X., Zhang, K. and Comstock, J. M.: Aerosol effects on cirrus through ice nucleation in the Community Atmosphere Model CAM5 with a statistical cirrus scheme, J. Adv. Model. Earth Syst., 6, 513–526, doi:10.1002/2014MS000339, 2014a.

Wang, Y., Liu, X., Hoose, C., and Wang, B.: Different contact angle distributions for heterogeneous ice nucleation in the Community Atmospheric Model version 5, Atmos. Chem. Phys., 14, 10411–10430, https://doi.org/10.5194/acp-14-10411-2014, 2014b.

Wofsy, S. C.: HIAPER Pole-to-Pole Observations (HIPPO): Fine-grained, global-scale measurements of climatically important atmospheric gases and aerosols, Philos. Trans. R. Soc. A Math. Phys. Eng. Sci., 369(1943), 2073–2086, doi:10.1098/rsta.2010.0313, 2011.

Wolf, V., Kuhn, T., Milz, M., Voelger, P., Krämer, M. and Rolf, C.: Arctic ice clouds over northern Sweden: Microphysical properties studied with the Balloon-borne Ice Cloud particle Imager B-ICI, Atmos. Chem. Phys., 18(23), 17371–17386, doi:10.5194/acp-18-17371-2018, 2018.

Wu, C., Liu, X., Diao, M., Zhang, K., Gettelman, A., Lu, Z., Penner, J. E. and Lin, Z.: Direct comparisons of ice cloud macro- and microphysical properties simulated by the Community Atmosphere Model version 5 with HIPPO aircraft observations, Atmos. Chem. Phys., 17(7), 4731–4749, doi:10.5194/acp-17-4731-2017, 2017.

Zhang, G. J. and McFarlane, N. A.: Sensitivity of climate simulations to the parameterization of cumulus convection in the canadian climate centre general circulation model, Atmos. - Ocean, 33(3), 407–446, doi:10.1080/07055900.1995.9649539, 1995.

Zhang, K., Liu, X., Wang, M., Comstock, J. M., Mitchell, D. L., Mishra, S. and Mace, G. G.: Evaluating and constraining ice cloud parameterizations in CAM5 using aircraft measurements from the SPARTICUS campaign, Atmos. Chem. Phys., 13(9), 4963–4982, doi:10.5194/acp-13-4963-2013, 2013.

Zhang, Y., MacKe, A. and Albers, F.: Effect of crystal size spectrum and crystal shape on stratiform cirrus radiative forcing, Atmos. Res., 52(1–2), 59–75, doi:10.1016/S0169-8095(99)00026-5, 1999.

Zhao, B., Liou, K.-N., Gu, Y., Jiang, J. H., Li, Q., Fu, R., Huang, L., Liu, X., Shi, X., Su, H. and He, C.: Impact of aerosols on ice crystal size, Atmos. Chem. Phys., 18, 1065–1078, doi:10.5194/acp-18-1065-2018, 2018.

Zhao, B., Wang, Y., Gu, Y., Liou, K. N., Jiang, J. H., Fan, J., Liu, X., Huang, L. and Yung, Y. L.: Ice nucleation by aerosols

from anthropogenic pollution, Nat. Geosci., doi:10.1038/s41561-019-0389-4, 2019.

Zhou, C., Penner, J., Lin, G., Liu, X. and Wang, M.: What controls the low ice number concentration in the upper troposphere?, Atmos. Chem. Phys., 16(19), 12411–12424, doi:10.5194/acp-16-12411-2016, 2016.

Zondlo, M. A., Paige, M. E., Massick, S. M. and Silver, J. A.: Vertical cavity laser hygrometer for the National Science Foundation Gulfstream-V aircraft, J. Geophys. Res. Atmos., 115(20), 1–14, doi:10.1029/2010JD014445, 2010.

725 **Table 1.** Descriptions of seven NSF flight campaigns conducted with the NSF/NCAR G-V research aircraft.

Acronym	Field Campaign	Time	Lat, Lon	Region*	Flight hours	In-cloud hours	Clear-sky hours
START08	Stratosphere-Troposphere Analyses of Regional Transport	April – June 2008	26°N – 62°N, 117°W – 86°W	NM, NP	84	2	52
HIPPO	HIAPER Pole-to-pole Observations deployments 2 – 5	Oct – Nov 2009; Mar – Apr 2010; Jun – July 2011; Aug – Sept 2011	87°N – 67°S, 128°E – 90°W	A	333	7	111
PREDICT	PRE-Depression Investigation of Cloud Systems in the Tropics	Aug – Sept 2010	10°N – 28.5°N, 86°W – 37°W	NT	105	25	66
DC3	Deep Convective Clouds and Chemistry Project	May – June 2012	25°N – 42°N, 106°W – 80°W	NM	144	23	54
TORERO	Tropical Ocean tRoposphere Exchange of Reactive halogen species and Oxygenated voc	Jan – Feb 2012	42°S – 14°N, 105°W – 70°W	NT, ST, SM	125	2	52
CONTRAST	CONvective TRansport of Active Species in the Tropics	Jan – Feb 2014	20°S – 40°N, 132°E – 105°W	NM, NT, ST	116	23	48
ORCAS	The O_2/N_2 Ratio and CO_2 Airborne Southern Ocean (ORCAS) Study	Jan – Mar 2016	75°S – 18°S, 91°W – 51°W	SM, SP	95	1	40

*: N, northern hemisphere; S, southern hemisphere; T, tropics; M, midlatitude; P, polar regions; A, all regions.

Table 2. Ranges of meteorological conditions and ice microphysical properties for in situ 1-Hz observations, 430-s averaged observations, CAM6-nudg and CAM6-free data used in this study.

	In situ observations	430-s averaged observations	CAM6-nudg	CAM6-free
T (ºC)	-78 – -40	-77 – -40	-75 – -40	-89.9 – -40
P (Pa)	12,389 – 53,137	37,778 – 53,410	12,300 – 53,446	12,300 – 53,100
RHi (%) in-cloud (clear sky)	0.99 – 175.1 (0.3 – 174.9)~~0.3 – 175.1~~	0.3 – 153.7 (0.3 – 134.6)	0.8 – 159.8 (0.05 – 107.6)~~0.0473 – 159.8~~	0.003 – 257.2 (0.001 – 181.4)~~0.002 – 257.19~~
IWC (g/m^3)	0.00004 – 23.31	1e-7 – 11.58	1e-7 – 0.12~~0.00001 – 32.65~~	1e-7 – 0.16~~0.00001 – 94.72~~
Ni (#/L)	0.039 – 542.15	9.6e-5 – 188.7	1e-4 – 207.04~~0.01 – 5,238~~	1e-4 – 516.7~~0.0243 – 6,066~~
Di (µm)	62.5 – 3200	62.5 – 2175	62.5 – 2062~~62.5 – 1,958~~	66.7 – 2556

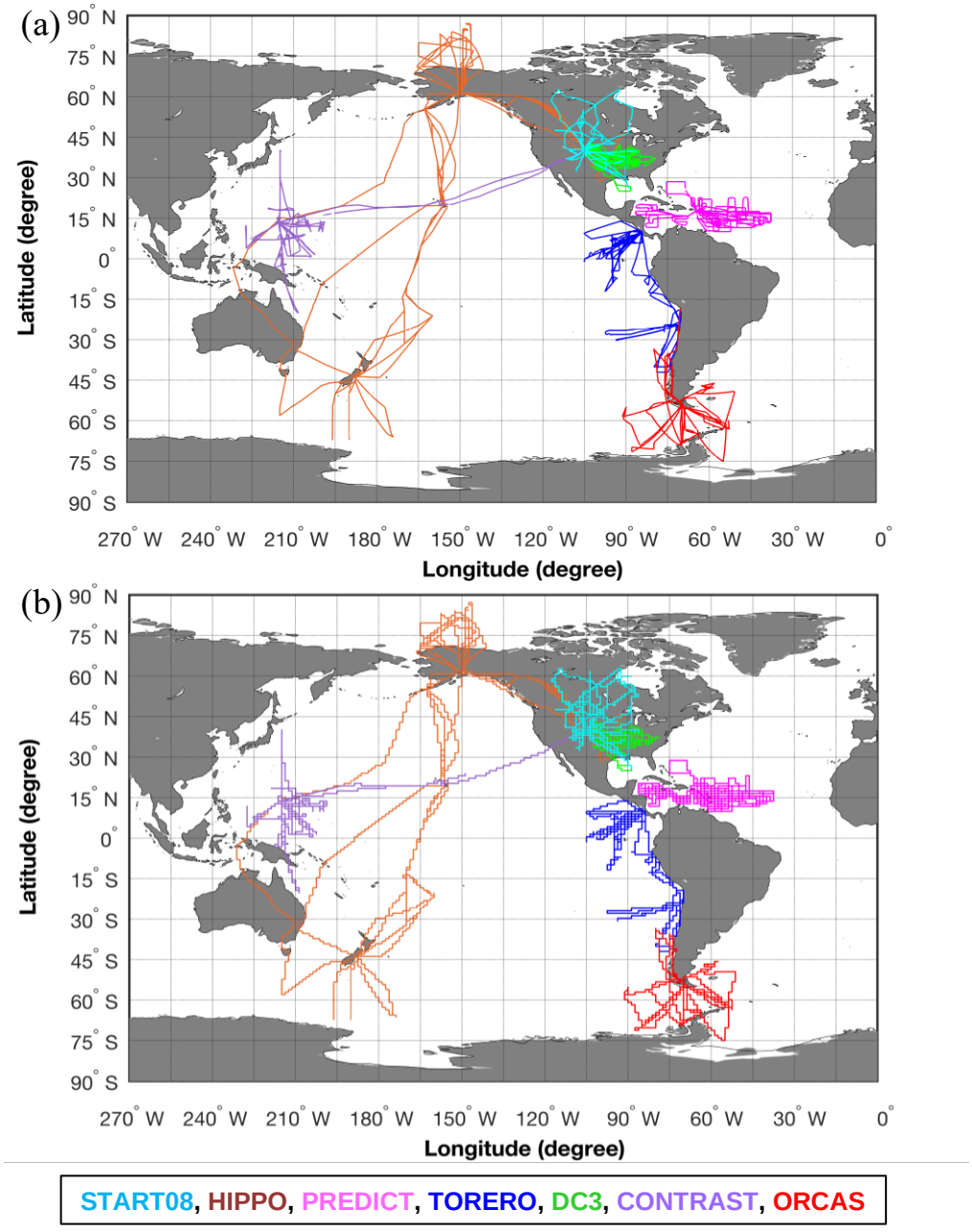

Figure 1. Global maps of flight tracks representing the seven campaigns in this study for (a) in situ observations and (b) CAM6-nudg. Colors denote different campaigns.

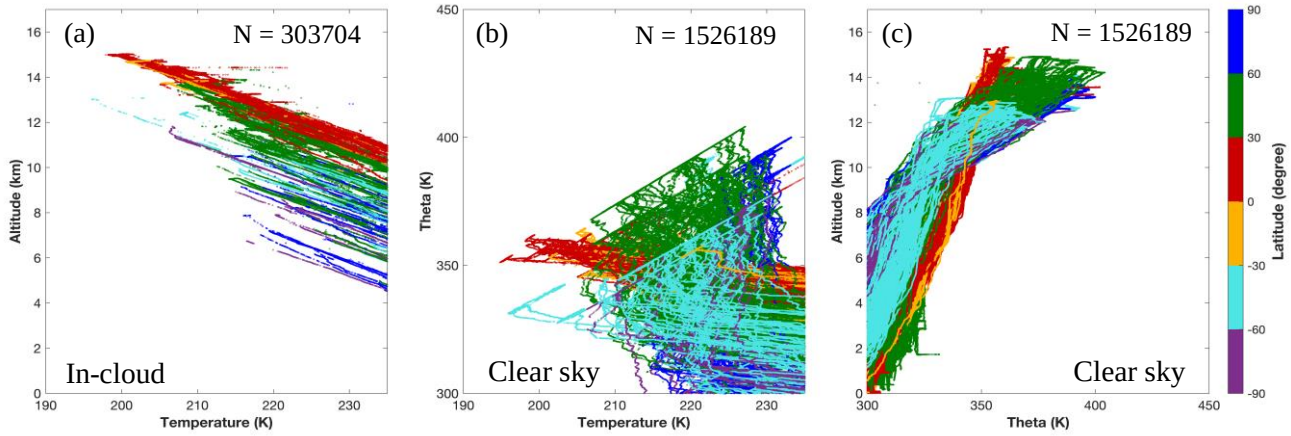

735

Figure 2. (a) Vertical profiles of temperature, (b) potential temperature vs. temperature, and (c) vertical profiles of potential temperature based on in situ observations at temperatures ≤ -40ºC. Number of samples (N) for 1-Hz observations is shown in the figure legend. Colors denote six latitudinal regions.

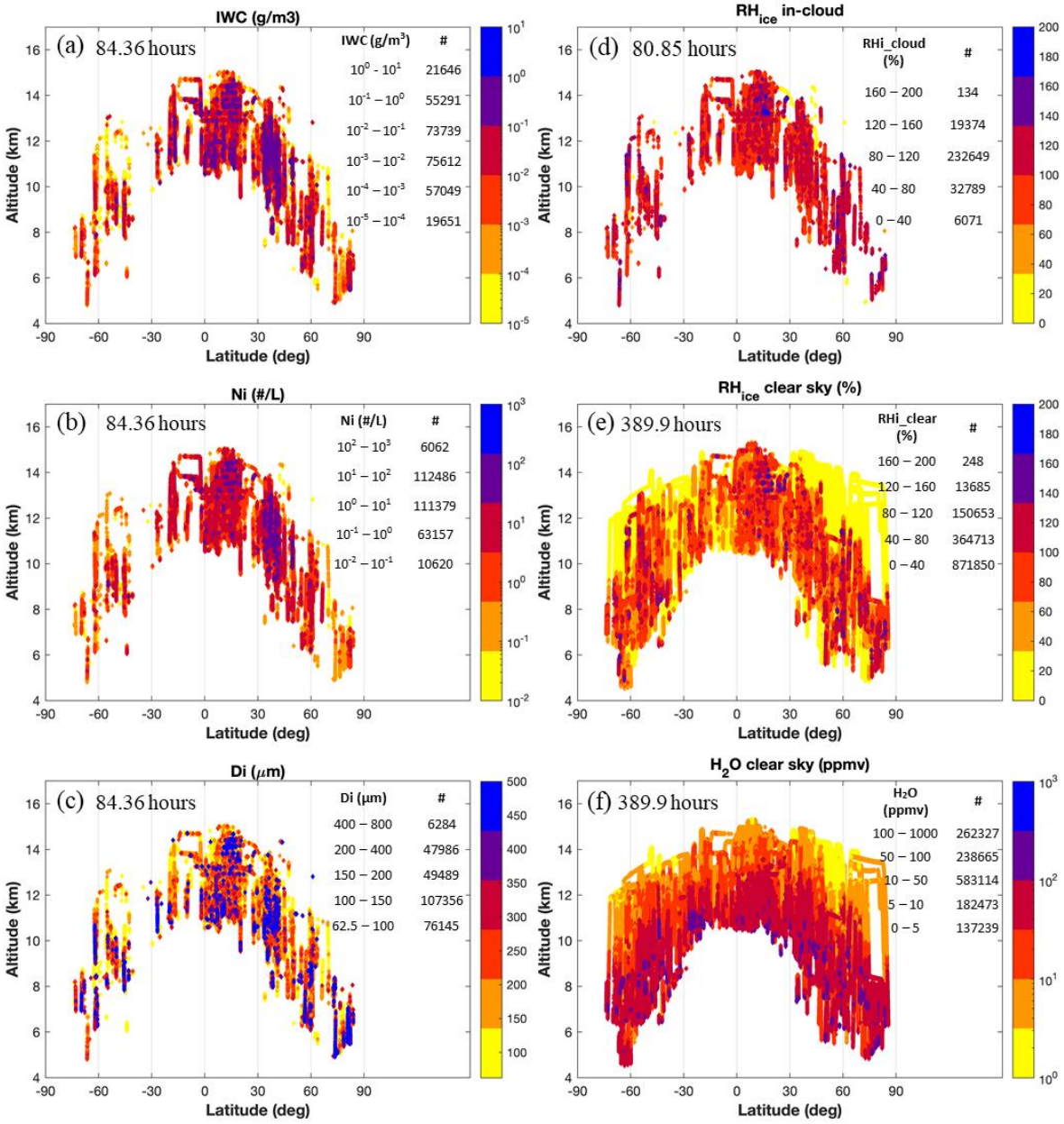

740 **Figure 3.** Latitude and altitude distributions of (a) IWC, (b) Ni, (c) Di, (d) in-cloud RHi, (e) clear-sky RHi, and (f) clear-sky water vapor volume mixing ratio at temperatures ≤ -40ºC. Total measurement hours and number of samples for given intervals are shown for each variable. Note that the measurement ranges shown in the upper right corner are not the full ranges (see Table 2 for the full ranges).

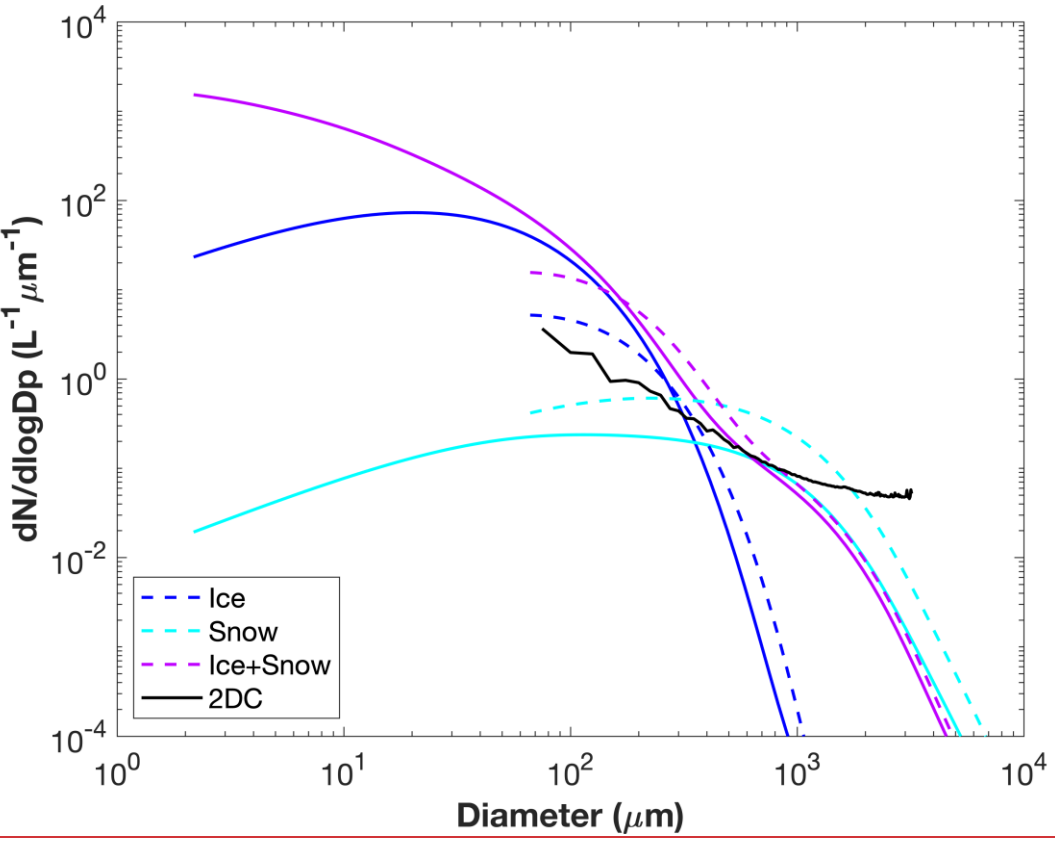

Figure 4. Observed size distribution (black line) and reconstructed size distributions from simulated ice (blue) and snow (cyan). Both full size range (solid lines) and truncated size range of diameters ≥ 62.5 μm (dashed lines) are shown for simulated hydrometeors. Size distributions for combined ice and snow in the simulations (purple) are also shown before and after the size restriction.

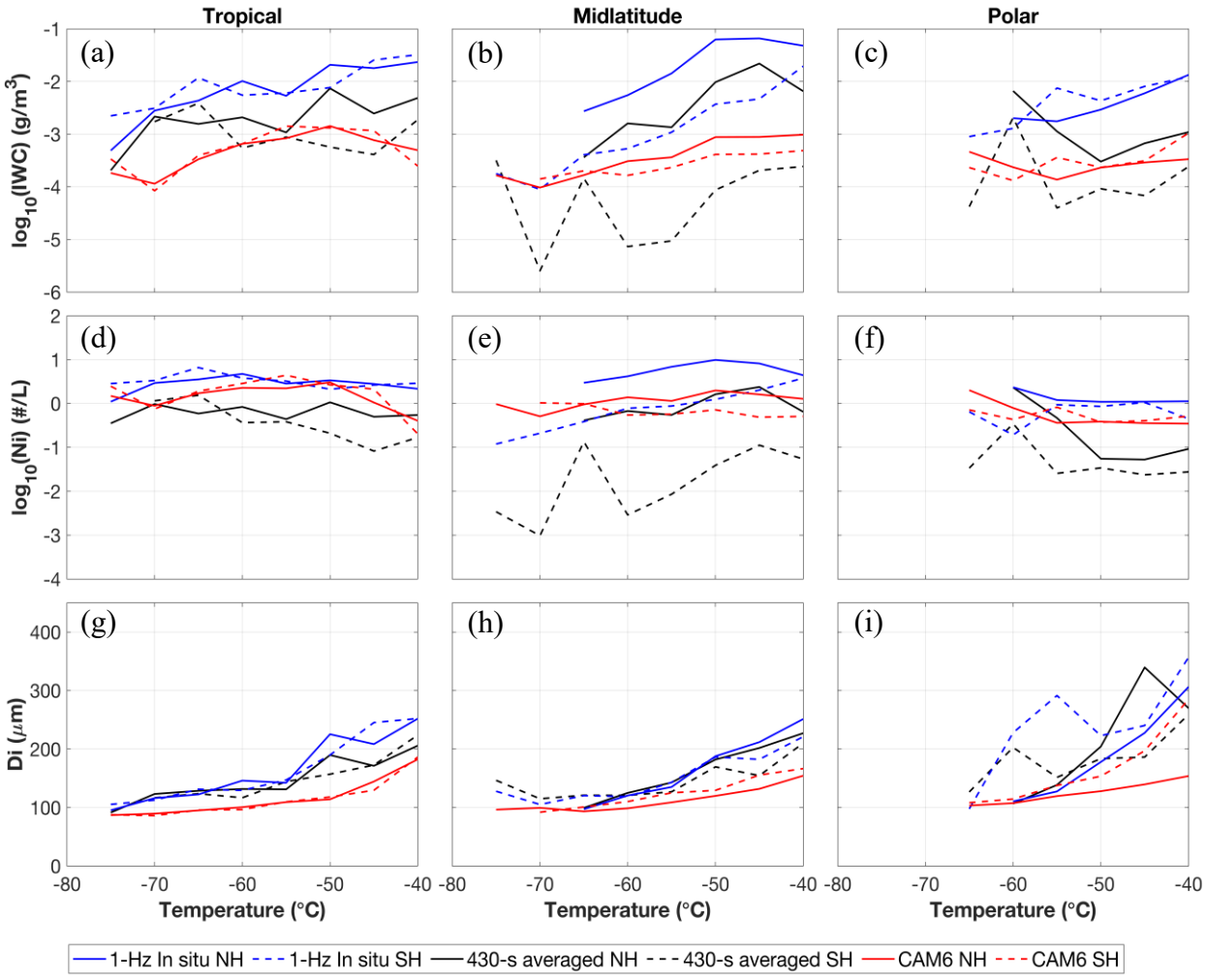

Figure 5. Geometric means of (a – c) IWC and (d – f) Ni, as well as (g – i) linear averages of Di at 5ºC temperature intervals between -80ºC and -40ºC, compared between 1-Hz in situ observations (blue lines), 430-s averaged observations (black lines) and CAM6-nudg (red lines). Observed and simulated microphysical properties are binned by six latitudinal regions, where NH is denoted by solid lines, and SH is denoted by dashed lines. The number of samples for 1-Hz observations at temperatures ≤ -40ºC in the northern (southern) hemisphere tropical, midlatitude and polar regions are 173930 (15569), 100615 (3809), and 6704 (2606), respectively. The number of samples for 430-s averaged observations in these regions are 355082 (40683), 233546 (26850) and 24083 (10252), respectively. The number of samples for CAM6-nudg data in these regions are 3241592 (653110), 2052353 (590503) and 478844 (209662), respectively.

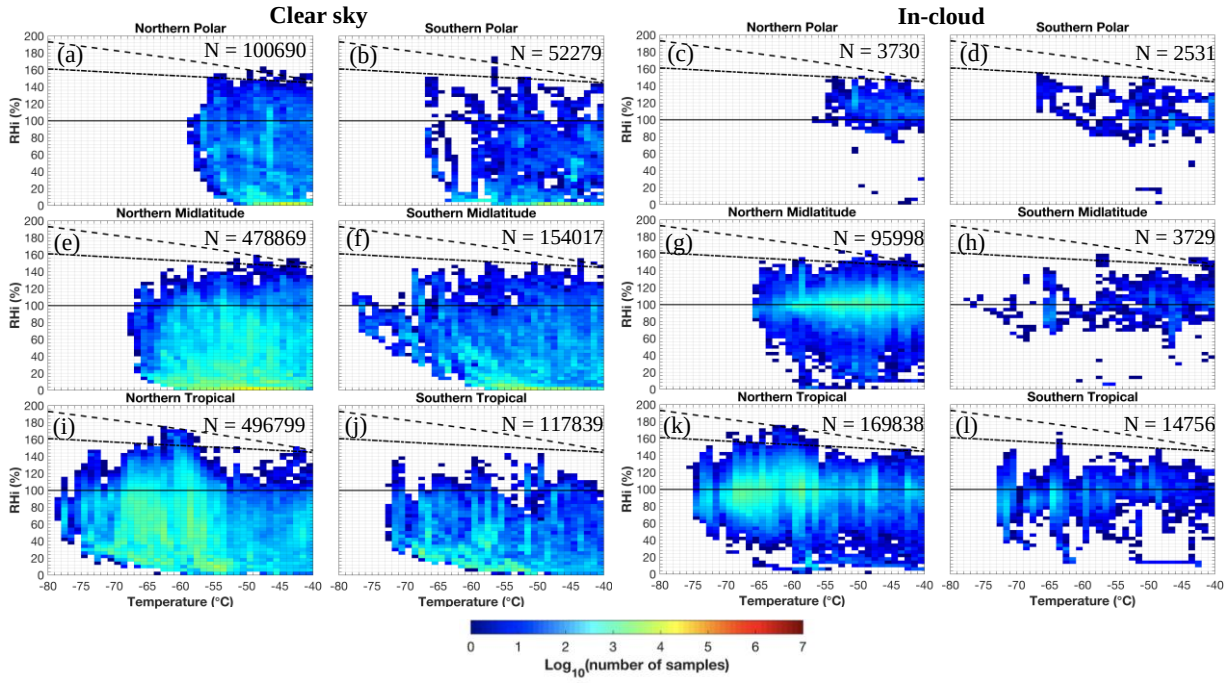

Figure 6. Distributions of RHi at various temperatures and geographical locations from in situ observations under (left two columns) clear-sky and (right two columns) in-cloud conditions. Solid and dashed black lines represent ice and liquid saturation, calculated based on saturation vapor pressure with respect to ice and liquid from Murphy and Koop (2005), respectively. Dash-dotted line denotes the homogeneous freezing threshold for 0.5 μm aerosols based on Koop et al. (2000).

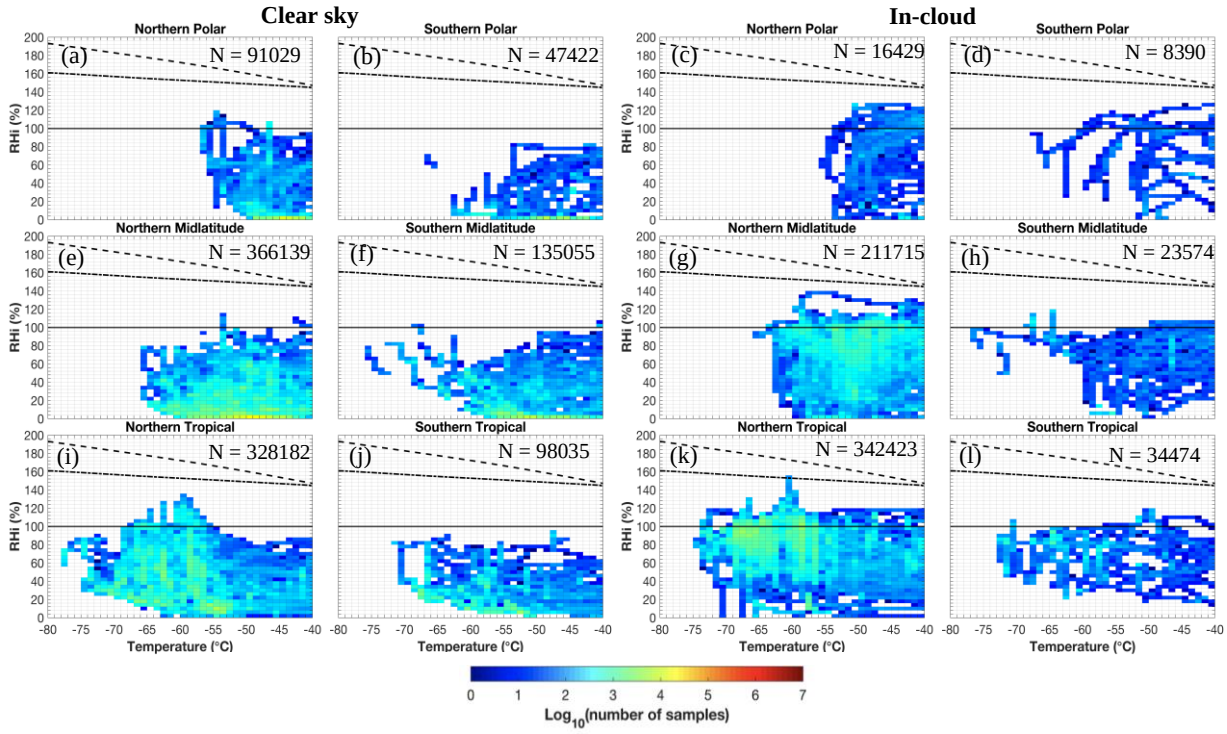

765

Figure 7. Similar to Figure 6 but for 430-s averaged observations.

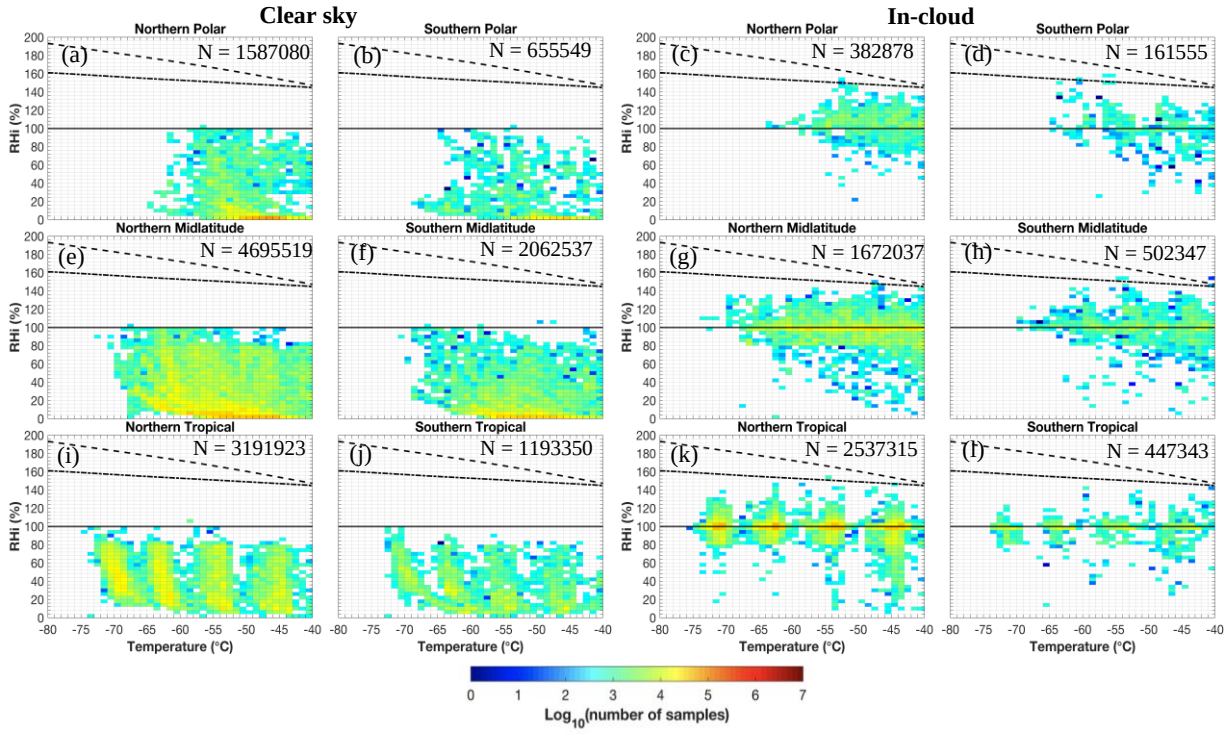

Figure 8. Similar to Figure 6 but for CAM6-nudg data. RHi values for simulations are calculated using simulated specific humidity and temperature, based on the equation of saturation vapor pressure with respect to ice from Murphy and Koop (2005).

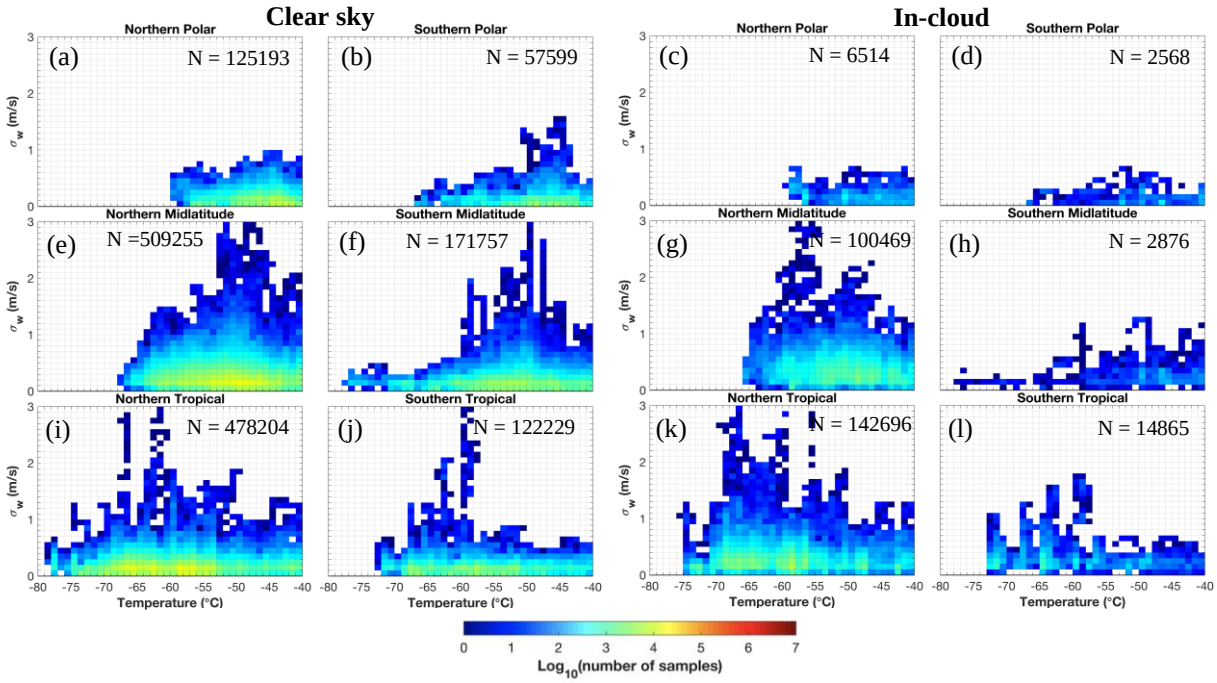

Figure 9. Distributions of σ_w calculated for every 40 seconds using the 1-Hz observations under (left two columns) clear-sky and (right two columns) in-cloud conditions.

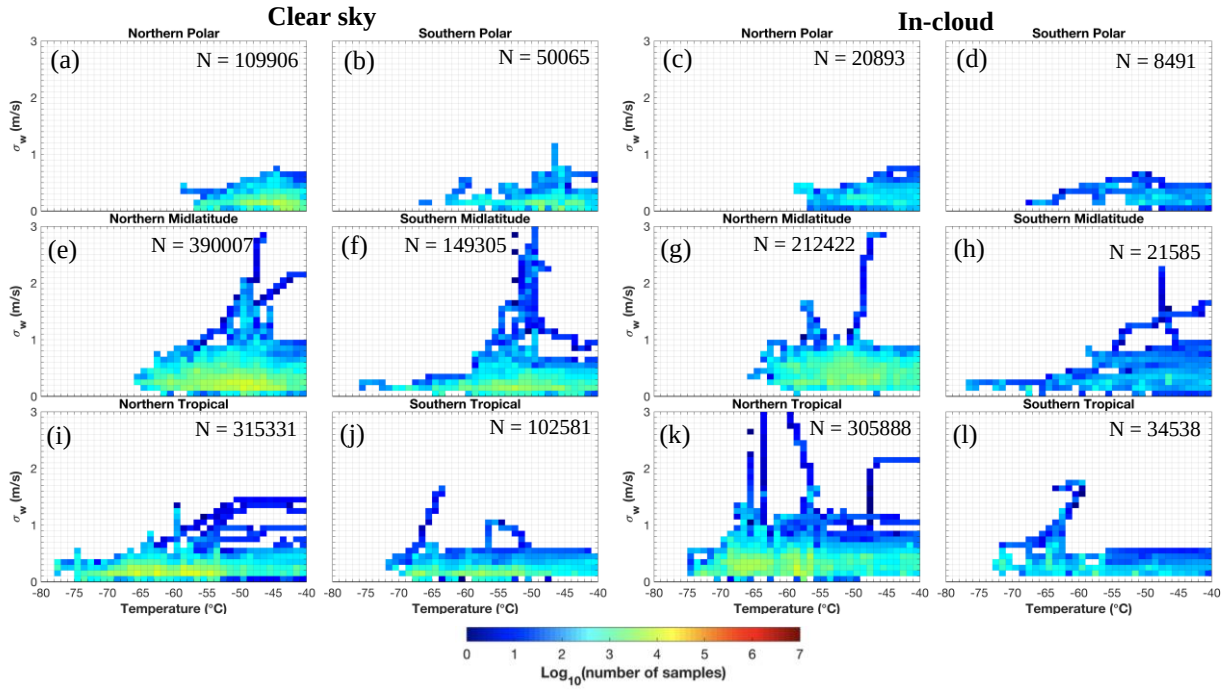

Figure 10. Similar to Figure 9, but for 430-s scale.

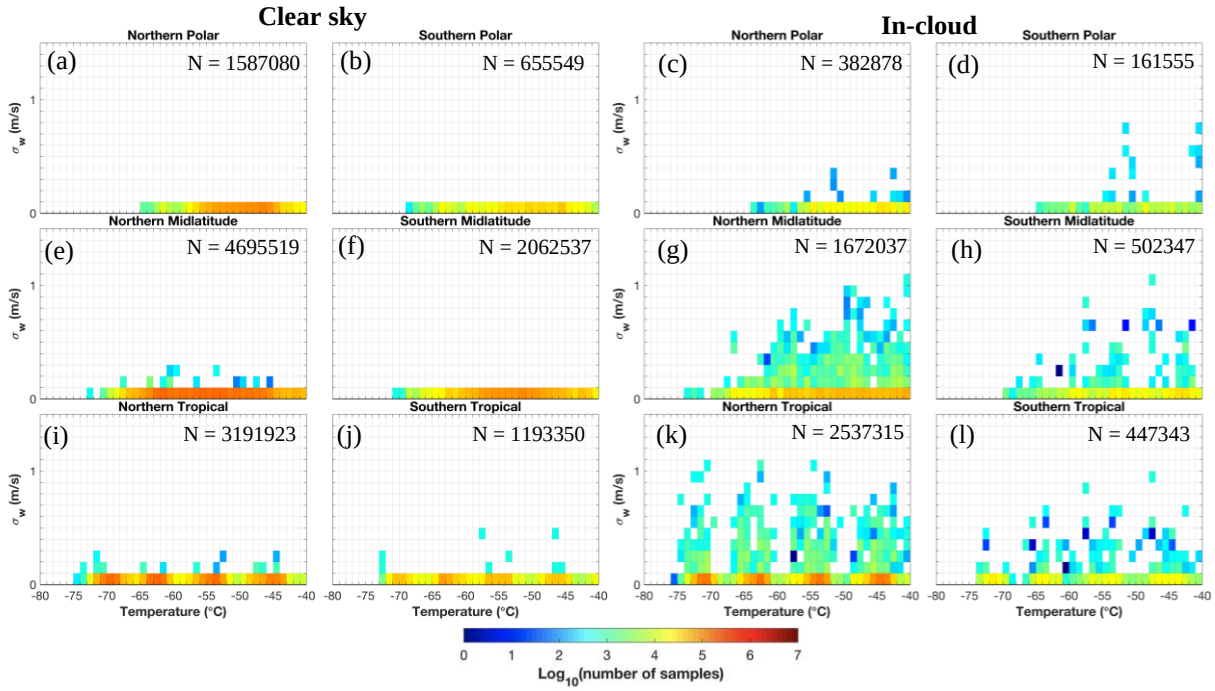

Figure 11. Similar to Figure 9 but for the CAM6-nudg data.

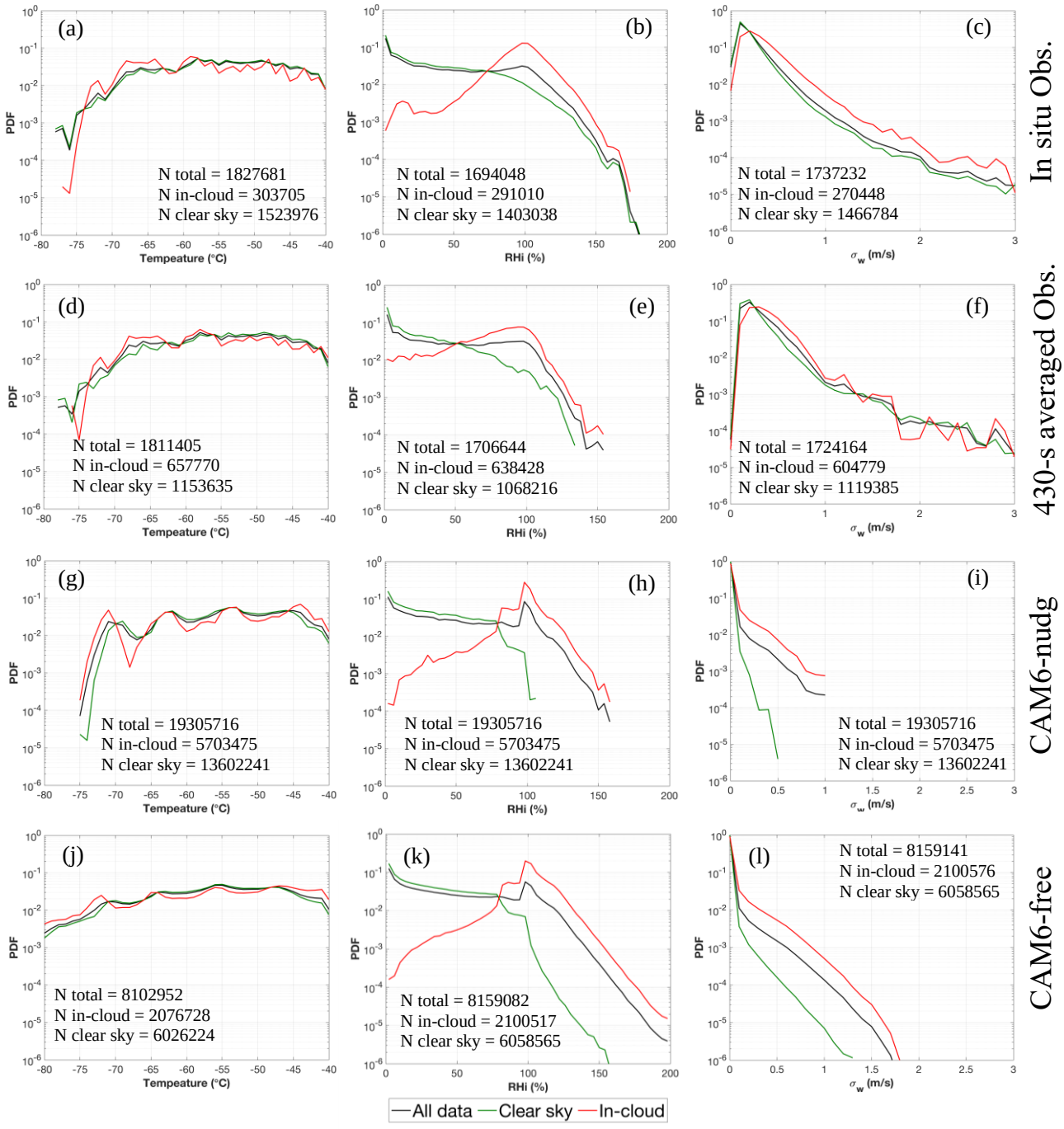

Figure 12. Probability density functions (PDFs) for (left column) temperature, (middle column) RHi and (right column) σ_w, compared among (a– c) 1-Hz observations, (d – f) 430-s averaged observations, (g – i) CAM6-nudg and (j - l) CAM6-free data. Note that σ_w in (c) is calculated for every 40 seconds.

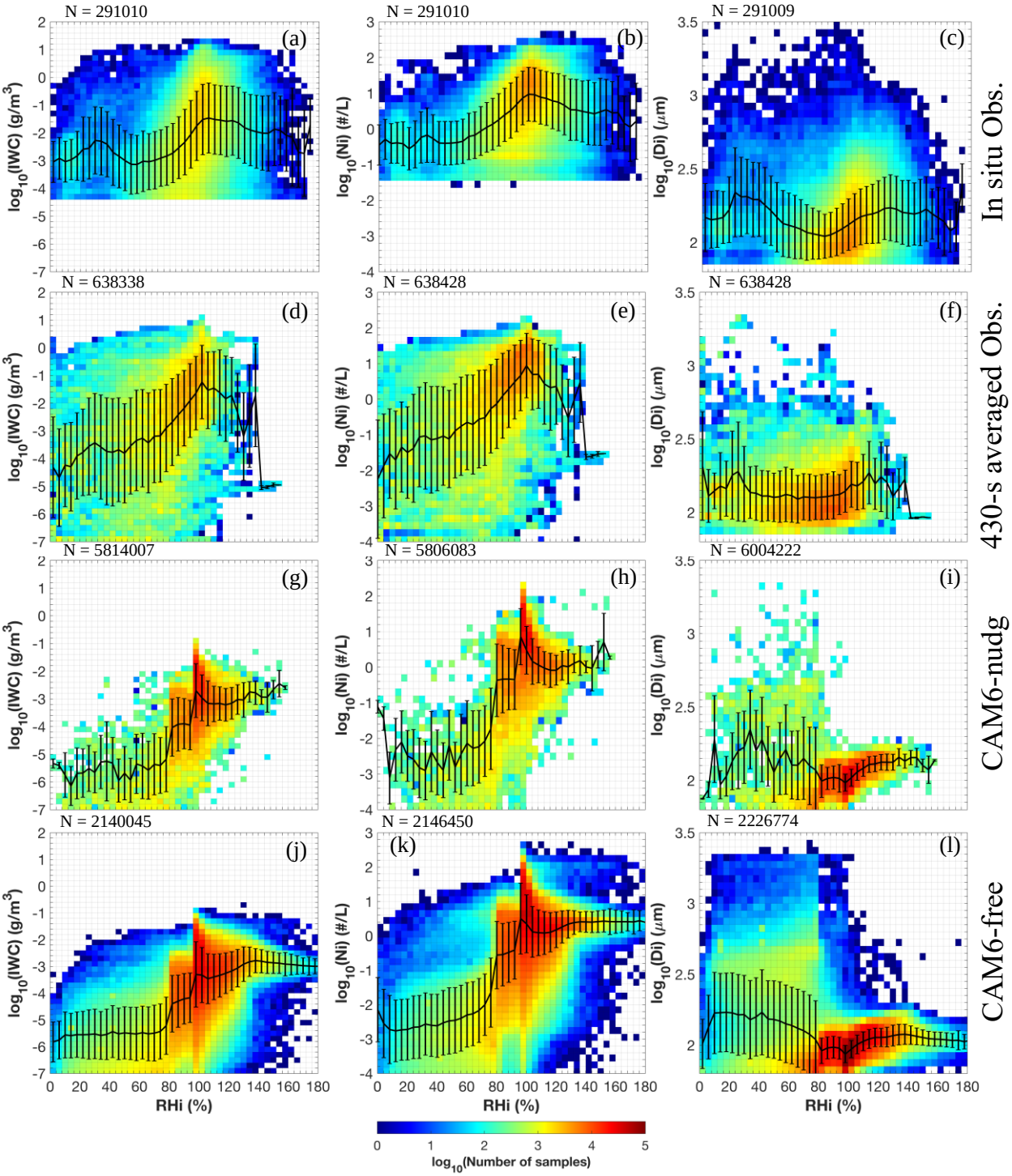
N = 291010
(a)
N = 291010
(b)
N = 291009
(c)
In situ Obs.
N = 638338
(d)
N = 638428
(e)
N = 638428
(f)
430-s averaged Obs.
N = 5814007
(g)
N = 5806083
(h)
N = 6004222
(i)
CAM6-nudg
N = 2140045
(j)
N = 2146450
(k)
N = 2226774
(l)
CAM6-free
log10(IWC) (g/m3)
log10(Ni) (#/L)
log10(Di) (μm)
RHi (%)
log10(Number of samples)

Figure 13. Correlations between RHi and in-cloud IWC, Ni and Di (columns 1 – 3, respectively), compared among (a – c) in situ 1-Hz observations, (d – f) 430-s averaged observations, (g – i) CAM6-nudg, and (j – l) CAM6-free data. Black lines and whiskers denote geometric means and standard deviations, respectively.

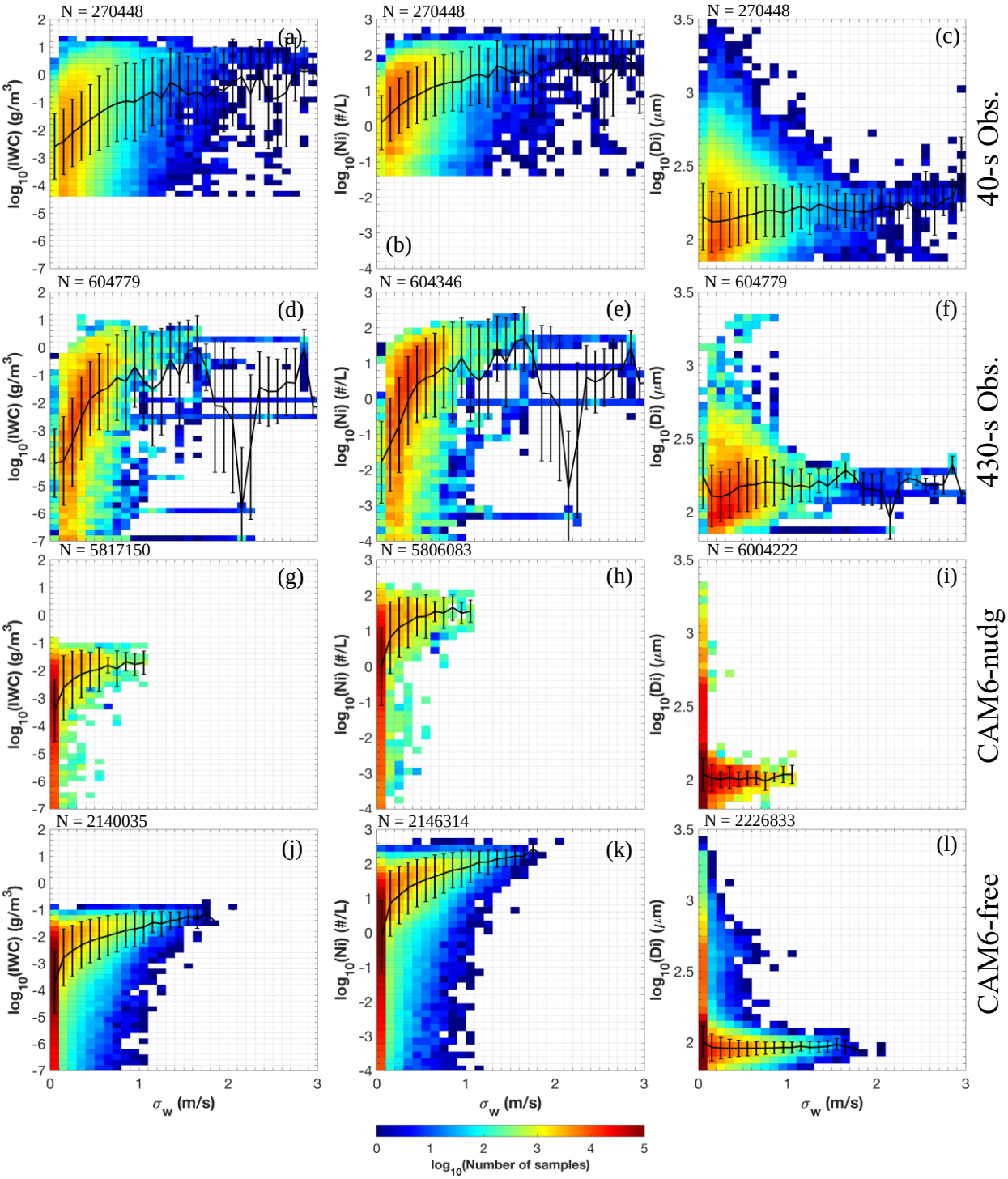

Figure 14. Similar to Figure 13 but for correlations with σ_w. Note that σ_w of observations are calculated for (a – c) every 40 seconds and (d – f) every 430 seconds using the 1-Hz observations.

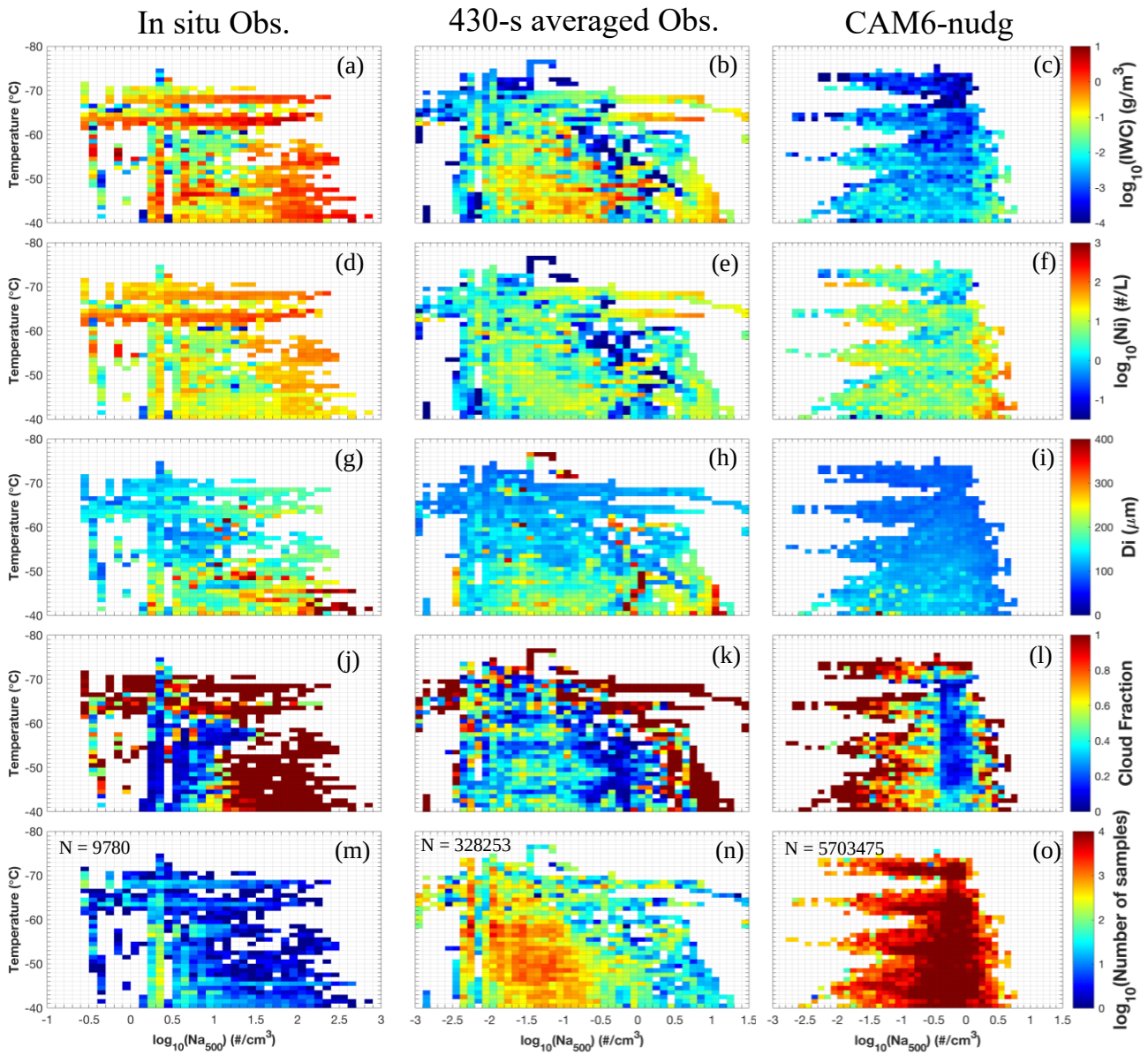

Figure 15. Aerosol indirect effects from logarithmic-scale Na_{500} on (a – c) IWC, (d – f) Ni, (g – i) Di, and (j – l) cloud fraction, compared among 1-Hz observations (left column), 430-s averaged observations (middle column) and CAM6-nudg data (right column). Number of samples of each bin is shown in the bottom row (m – o). Cloud fraction is calculated as the number of in-cloud samples over the total number of samples for a given temperature and Na bin.

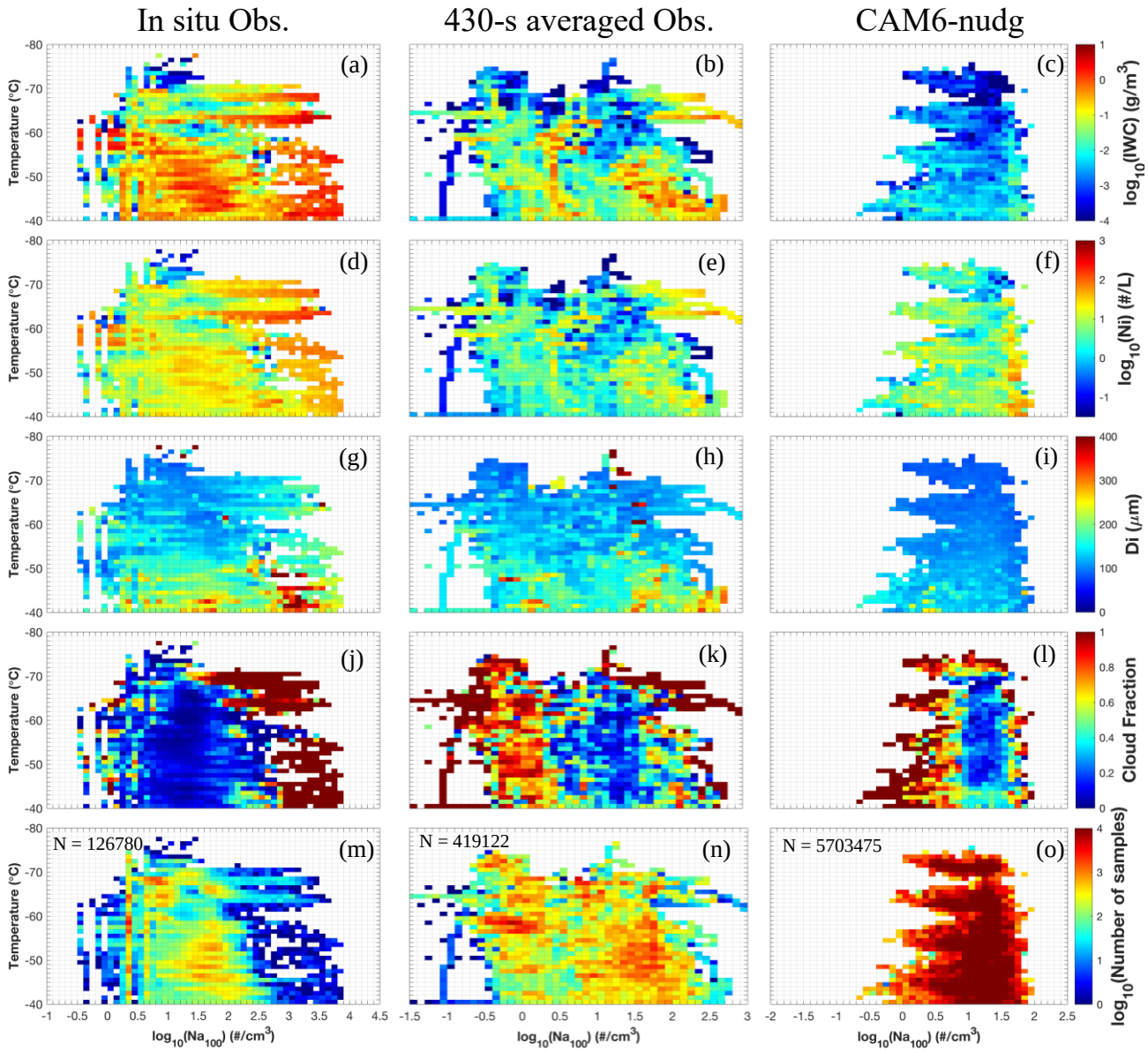

795

Figure 16. Similar to Figure 15, but examined for $\log_{10}(Na_{100})$.